Journal of Geophysical Research: Earth Surface

RESEARCH ARTICLE
10.1029/2017JF004575

Variable-Threshold Behavior in Rivers Arising From Hillslope-Derived Blocks

Charles M. Shobe[1], **Gregory E. Tucker**[1], **and Matthew W. Rossi**[2]

[1]Cooperative Institute for Research in Environmental Sciences and Department of Geological Sciences, University of Colorado, Boulder, CO, USA, [2]Earth Lab, University of Colorado, Boulder, CO, USA

Key Points:
- Modeling suggests that hillslope-derived blocks steepen channels across a wide range of erosion rates and climatic conditions
- Block effects may be incorporated into simple channel evolution models as an erosion threshold that varies with erosion rate
- Variable-threshold models predict unique relationships between erosion rate and channel steepness

Supporting Information:
- Supporting Information S1

Correspondence to:
C. M. Shobe,
charles.shobe@colorado.edu

Citation:
Shobe, C. M., Tucker, G. E., & Rossi, M. W. (2018). Variable-threshold behavior in rivers arising from hillslope-derived blocks. *Journal of Geophysical Research: Earth Surface*, *123*, 1931–1957. https://doi.org/10.1029/2017JF004575

Received 1 DEC 2017
Accepted 19 JUN 2018
Accepted article online 13 JUL 2018
Published online 22 AUG 2018

Abstract Geomorphologists often rely on simple models of river channel incision for predicting rates of landscape evolution and channel response to perturbations, as well as extracting climatic and tectonic signals from river longitudinal profiles. Recent work has shown that large, hillslope-derived blocks delivered to rivers may noticeably alter the form and evolution of river profiles from the behavior predicted by the most common models. Here we use a 1-D model of river reach erosion and hillslope block delivery to explore the conditions under which block delivery strongly influences channel evolution. We use global sensitivity analysis to understand which model parameters most strongly affect the channel longitudinal profile. We explore the effects of blocks on the relationship between erosion rate and channel gradient, and on the erosion rate-channel steepness exponent ϕ, and find that block effects result in highly variable slope and ϕ over the range of erosion rates and climatic conditions (discharge mean and variability) tested. The influence of blocks on erosion rate-slope scaling may be approximated by a piecewise model: The erosion threshold imposed by blocks scales linearly with erosion rate when blocks are infrequently mobile and remains constant when blocks are frequently mobile. We explore the implications of this variable-threshold model for the erosion rate-channel steepness relationship and find that erosion rate-dependent thresholds imposed by hillslope-derived blocks cause significant departures from previous models but may be consistent with existing field data sets. Our work has implications for landscape evolution modeling and the inversion of channel profiles for forcing information.

Plain Language Summary Rivers control how quickly mountain ranges erode. The amount, size, and durability of sediment delivered to rivers determine the shape of their channels and control how rapidly those channels cut through bedrock. Studies of river erosion tend to focus on how rivers respond to the delivery of smaller sediment like sand or gravel. But steep mountain hillslopes often deliver larger sediment, including boulders and blocks of rock, into river valleys. In this study, we used a mathematical model of river erosion to explore river response to the delivery of these larger blocks to the channel. We found that the rate of block delivery, the durability of the blocks, and the block size strongly controlled the slope of rivers. We also found that block delivery to rivers fundamentally changed the relationship between how quickly a landscape was eroding and how steep that landscape was. Quantifying how block delivery affects river erosion will help mitigate natural hazards and aid prediction of future changes to Earth's surface.

1. Introduction and Background

Fluvial erosion governs the topographic evolution of much of the Earth's surface (e.g., Burbank et al., 1996; Whipple, 2004), controls the longevity of landforms (e.g., Anderson, 1994; Baldwin et al., 2003; Bonetti & Porporato, 2017; Egholm et al., 2013; Hobley et al., 2010), and transmits tectonic and climatic perturbations through drainage networks (e.g., Tucker & Slingerland, 1997; Whipple et al., 2017). The manner in which erosion, deposition, and transport of sediment influence river erosion remains inadequately understood. Our understanding of the role of very large sediment grains (blocks of rock) in river erosion is especially poor, as most previous field, modeling, and experimental studies focus on mobile sediment fractions with transport dynamics measurable on human timescales. However, pioneering field geologists speculated on the outsized role that the largest grains play in channel and landscape evolution (Gilbert, 1877; Hack, 1965). The questions raised by their observations still stand (e.g., Attal, 2017; Howard et al., 1994). Does the presence of blocks significantly alter fluvial processes on landscape evolution timescales? How do blocks affect channel form and topographic outcomes?

Numerous modeling studies have explored the problem of river incision into bedrock (see reviews by Hobley et al., 2011; Lague, 2014; Shobe et al., 2017; Turowski, 2018). The most basic shear stress/stream power models cast vertical river incision as a function of water quantity (discharge, flow depth, or drainage area) and channel slope, without accounting explicitly for the effects of sediment (e.g., Howard, 1994; Whipple & Tucker, 1999). Such models may be augmented to include erosion thresholds and stochastic distributions of flood events, thereby improving model fits to natural landscapes in some field areas (Attal et al., 2011; DiBiase & Whipple, 2011; Lague et al., 2005; Scherler et al., 2017; Snyder et al., 2003; Tucker, 2004; Tucker & Bras, 2000). Incorporating a dependence of river incision on sediment flux allows parameterized or explicit representation of the "tools" and "cover" effects, in which the presence of sediment may increase or reduce the efficiency of river incision (e.g., Gasparini et al., 2006; Lague, 2010; Sklar & Dietrich, 1998, 2004; Shobe et al., 2017; Turowski, 2009, 2018; Turowski & Hodge, 2017; Turowski et al., 2007; Whipple & Tucker, 2002; Zhang et al., 2015). In sediment flux-dependent incision models, the grain size distribution is commonly either represented by a single median or characteristic grain size value (e.g., Gasparini et al., 2006; Hobley et al., 2011; Sklar & Dietrich, 2004) or divided into several grain-size bins across which the erosive effects of each size fraction are summed (e.g., Egholm et al., 2013; Sklar & Dietrich, 2006).

Grain size strongly influences fluvial erosion in both transport- and detachment-limited settings (see brief review by Sklar et al., 2016). At the reach scale, grain size has been shown to set the hydraulic roughness (e.g., Ferguson, 2007) and the relative importance of the tools and cover effects (Johnson, 2014; Lamb, Dietrich, & Sklar, 2008; Scheingross et al., 2014; Sklar & Dietrich, 2004; Turowski & Rickenmann, 2009). At larger spatial and temporal scales, grain size influences channel width (Finnegan et al., 2007), slope (Finnegan et al., 2017; Johnson et al., 2009; Sklar & Dietrich, 2006), and adjustment timescales (Cook et al., 2013; Egholm et al., 2013). Despite the strong influence of sediment size on channel morphodynamics and long-term landscape evolution, the simplifications inherent to many fluvial erosion models disregard the full range of grain sizes. Egholm et al. (2013) used a maximum grain size of 256 mm when modeling postorogenic landscape decay driven by river erosion and landsliding. This value is only 70% of the maximum grain size delivered by landslides to the Marsyandi River (Attal & Lavé, 2006) and is much smaller than the meter to several meter-scale blocks observed in channels elsewhere (e.g., Bennett et al., 2016; Shobe et al., 2016; Thaler & Covington, 2016). Modelers often avoid explicitly modeling fluvial transport of large grains due to the reduced applicability of continuum sediment transport theory.

Several field studies have shown that the largest sediment grains found in fluvial networks may play an important role in altering the course and pace of landscape evolution. Seidl et al. (1994) found in Hawaii that many channel reaches below knickzones are mantled with boulders and speculated that boulder mantling makes river incision in these settings dependent on rates of boulder degradation and transport. Johnson et al. (2009) showed that channels incising sandstone in the Henry Mountains are steeper when diorite boulders are abundant on the channel bed than when the boulders are absent. DiBiase et al. (2015) noted clusters of large blocks in and below knickzones in the San Gabriel Mountains and hypothesized that hillslope fracture spacing dictates the in-channel distribution of large, bed-armoring grains. In the Feather River basin, Attal et al. (2015) observed that fluvial sediment is enriched in large grains within and below knickzones and argued that the largest grains are hillslope derived. Bennett et al. (2016) found exceptionally high channel steepness indices in channels bound by landslide-prone hillslopes and argued that bed armoring by resistant blocks of landslide-derived rock may inhibit knickpoint propagation and landscape adjustment. Working in a tectonically quiescent setting, Thaler and Covington (2016) found a strong positive correlation between channel steepness and both the size of in-channel boulders and percent of bed covered by boulders. DiBiase et al. (2018) argued that increased coarse sediment delivery to channels in the Northern San Jacinto Mountains relative to those in the San Gabriel Mountains substantially increases fluvial erosion thresholds and channel steepness. Taken together, these data suggest a strong influence of large blocks on river and landscape morphology over large spatial and temporal scales and throughout a wide range of environmental and geologic conditions. However, field data alone do not provide a mechanistic link between large blocks and channel morphology.

If blocks are not immediately mobile, they spend time shielding the channel bed from erosion by acting as bed cover. Blocks also act as large obstacles in the flow, causing frictional losses of erosive power through form drag. Theoretical, field, and experimental studies in the tradition of Einstein and Barbarossa (1952) confirm that large grains inhibit bed load transport and potentially bedrock incision (e.g., Chatanantavet & Parker, 2008; Ferguson, 2012; Johnson et al., 2009; Kean & Smith, 2006, 2010; Schneider et al., 2016; Shobe et al., 2016;

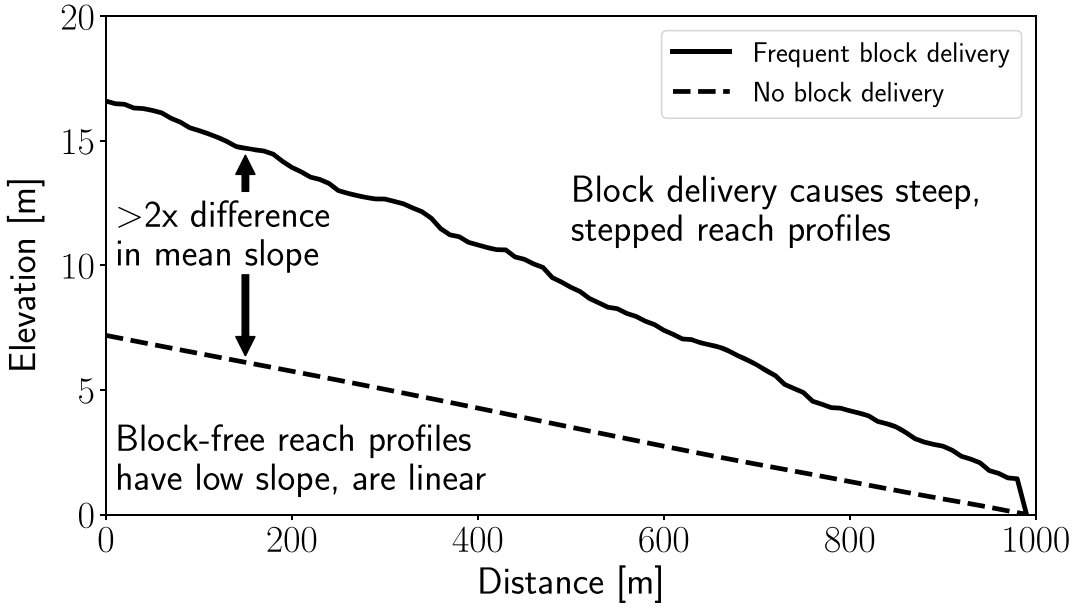

Figure 1. Demonstration of the general influences of hillslope-derived blocks on modeled channel reach longitudinal profile evolution. The reach is a length of river short enough to have constant drainage area. In the absence of blocks, a reach equilibrated to the erosion rate imposed at the outlet will therefore have a linear longitudinal profile (dashed line). Reach profiles are shown after 400 kyr of simulation time from the same initial condition using the modified Shobe et al. (2016) model for channel profile evolution in the presence of hillslope-derived blocks. The block-influenced profile (solid line) is over twice as steep as the no-blocks case (dashed line) and shows a characteristic stepped channel profile. The details of the model are presented in section 2.

Yager et al., 2007). Recently, Shobe et al. (2016) explicitly incorporated the effects of large, hillslope-derived blocks into a 1-D shear stress-based model of bedrock channel incision. They modeled a set of feedbacks in which rapid river incision steepens adjacent hillslopes and causes the delivery of large blocks, which then inhibits further erosion through bed cover and form drag effects. Shobe et al. (2016) found that incorporating block delivery feedbacks resulted in (1) channel reach longitudinal profiles that were steeper on average than those without block delivery (Figure 1), (2) highly variable slopes along block-influenced channel profiles, with local slope set by the presence or absence of blocks, and (3) a lack of correspondence between local channel slope and long-term erosion rate, indicating potential complications when extracting tectonic signals from block-influenced channels (their Figure 2, summarized here in Figure 1). The field observations of Seidl et al. (1994), Johnson et al. (2009), DiBiase et al. (2015), Bennett et al. (2016), Thaler and Covington (2016), Shobe et al. (2016), and DiBiase et al. (2018) suggest that such outcomes occur in some rivers, but we lack general theory for the effects of blocks on channel evolution.

We seek to explore theoretically the influence of large blocks delivered from hillslopes to river channels on long-term river channel evolution and the relationship between erosion rate and channel steepness. We ask four questions. First, which natural factors dominate the effects of blocks on channel evolution? We use a global sensitivity analysis of a previously published 1-D channel evolution model that combines the effects of blocks on bed cover and frictional energy losses (Shobe et al., 2016) to understand the conditions required for blocks to influence channel evolution. Second, how does block delivery alter the relationship between erosion rate and channel slope? We show that the influence of blocks on channel slope varies significantly but predictably over the range of erosion rates and climatic conditions we test. Third, how can the complex effects of hillslope-derived blocks be incorporated into landscape evolution models? We argue that the effects of large blocks on river morphology can be successfully captured by the inclusion of a threshold shear stress term that varies with erosion rate. Fourth, what are the implications of this variable-threshold model for topographic scaling in river channels? We explore the erosion rate-channel steepness relationships predicted by our variable-threshold block model and make comparisons with existing models and previously published field data.

2. Model Description

We use a modified version of the 1-D reach-scale numerical model of Shobe et al. (2016), which calculates fluvial erosion while accounting for the effects of large blocks supplied by the adjacent hillslopes. The model uses a modified shear stress bedrock erosion rule in conjunction with probabilistic delivery of large blocks from the adjacent hillslopes to the channel. The model domain is a river reach assumed short enough to have constant drainage area, uniform channel width, and uniform water discharge. Below we describe the model formulation and note several changes between the implementation used by Shobe et al. (2016) and the one we use here.

2.1. Fluvial Erosion

The model calculates the vertical river erosion rate ε in the presence of cubic, hillslope-derived blocks using a modified threshold shear stress rule (Howard, 1994; Howard & Kerby, 1983; Tucker, 2004). The efficiency of fluvial erosion is dictated by the amount of available shear stress above the critical shear stress for bedrock erosion after accounting for the shear stress exerted on in-channel blocks:

$$\varepsilon = k_b \left(\tau - \left(\tau_c + \tau_{\text{block}}\right)\right)^a (1 - f_c), \tag{1}$$

where k_b is a bed erodibility constant, τ is total available boundary shear stress given by the depth-slope product, τ_c is the critical bed shear stress required for bedrock erosion to occur, τ_{block} is the shear stress exerted on blocks, and a is an exponent. k_b, τ_c, and a are spatially and temporally uniform constants. The bed erodibility constant k_b incorporates the influence of climate, local hydrology, sediment dynamics, lithology, fracture density, and the relative importance of different bedrock erosion processes (e.g., plucking versus abrasion; Whipple, Hancock, & Anderson, 2000). While the exponent a may depend on the specific mechanics of bedrock erosion at a given site, we use a constant value of 1, which is both physically plausible (Hancock et al., 1998; Whipple, Hancock, & Anderson, 2000; Whipple & Tucker, 1999) and eliminates nonlinear effects that would hamper analysis of model results. The cover term f_c is the fraction of the bed covered by blocks of rock (the model does not incorporate bed or suspended load fluxes); $(1 - f_c)$ is therefore the fraction of the bed exposed to erosion (Sklar & Dietrich, 2004). We adapt the framework of Kean and Smith (2004, 2010) and Smith (2004), originally developed for fields of plant stems, to treat blocks as large roughness elements. The shear stress exerted on in-channel blocks τ_{block} is

$$\tau_{\text{block}} = \frac{\rho_w g h S \sigma_D}{1 + \sigma_D}, \tag{2}$$

where ρ_w is water density, g is gravitational acceleration, h is flow depth, S is local bed slope, and σ_D is a dimensionless drag stress. As with many simplified channel evolution models, we assume that the slope of the water surface closely approximates the bed slope. This simplification precludes the development of any bed topography that requires increasing bed elevation in the downstream direction, including waterfall plunge pools (e.g., Scheingross & Lamb, 2016) and step-pool sequences (e.g., Saletti et al., 2016). σ_D, the dimensionless drag stress on all blocks in the model cell, is given by

$$\sigma_D = \frac{1}{2} C_D \beta^2 \frac{h_b D}{\lambda^2}. \tag{3}$$

C_D is the drag coefficient of a cube (0.8; Carling & Tinkler, 1998), h_b is the average depth to which blocks are submerged (equal to block height for submerged blocks and equal to flow depth h for blocks protruding above the flow), D is average block side length (all blocks are cubes with volume D^3), and λ is the mean spacing of blocks. While there is no explicit connection between λ and f_c, the two quantities generally vary inversely with one another such that a higher spatial density of blocks results in more bed cover and vice versa. This approach to calculating form drag on blocks is similar to the one developed by Yager et al. (2007). Departing from the formulations used by both Smith (2004) and Yager et al. (2007), our model calculates the dimensionless roughness coefficient β and flow depth h using the variable power equation (VPE) of Ferguson (2007):

$$h = \frac{q}{u_* \beta} = \frac{q}{u_*} \frac{\left[(h/z_0)^{5/3} + (a_1/a_2)^2\right]^{1/2}}{a_1 (h/z_0)}. \tag{4}$$

The VPE was chosen because it has been shown to be appropriate for a wide range of roughness conditions, ranging from roughness elements much smaller than the flow depth to those whose size exceeds the flow depth (Ferguson, 2007, 2012, 2013). The VPE outperforms more traditional roughness relations most significantly in shallow, rough flows (Ferguson, 2013). q is discharge per unit channel width w in square meters per second ($q = Q/w$), u_* is shear velocity calculated as $\sqrt{ghS}$, a_1 and a_2 are constants set to 6.5 and 2.5, respectively (Ferguson, 2007), and z_0 is a roughness length scale that remains spatially and temporally constant. While the presence of large numbers of blocks may influence z_0, we do not have a defensible physical basis for a relationship between block size, number of blocks, and z_0. We therefore treat z_0 as background roughness of the bed surface while allowing blocks to inhibit erosion through bed cover and form drag.

Shobe et al. (2016) forced the model with the daily discharge record from Boulder Creek, CO. We instead draw from a Weibull discharge frequency distribution following Rossi et al. (2016). The probability distribution function of volumetric water discharge Q is

$$\mathrm{PDF}(Q) = \frac{c}{X_0}\left(\frac{Q}{X_0}\right)^{c-1} e^{-(Q/X_0)^c} \tag{5}$$

where

$$X_0 = \frac{\overline{Q}}{\Gamma\left(1+\frac{1}{c}\right)} \tag{6}$$

and Γ is the gamma function. The discharge distribution is described by the mean discharge $\overline{Q}$ and a shape parameter c. The exceedance probability of Q is a stretched exponential distribution that simplifies to the exponential distribution when $c = 1$ (see the supporting information). For $0 < c < 1$, the stretched exponential is more variable than the exponential distribution. For $c > 1$, the distribution is less variable than the exponential distribution (Rossi et al., 2016). We use c here to characterize the variability of streamflow. Because the numerical model simulates a single channel reach, we convert volumetric water discharge Q to discharge per unit width q by $q = Q/w$ where w is a constant channel width along the reach. For our numerical experiments we vary $\overline{Q}$ between 10 and 30 m^3/s and discharge variability c between 0.25 and 1.5. We use $\overline{Q} = 15\ m^3/s$ and $c = 0.5$ for all model runs unless otherwise stated. Our model does not incorporate an independent storm duration but instead has each flow event last for a fixed duration dt. Right-skewed distributions such as the inverse gamma (Lague et al., 2005) and stretched exponential are well suited to modeling daily streamflow or peak annual flow and thus serve as probability distribution functions that are appropriate for event-scale runoff variability. While we run our model at time steps of 10 years in order to simulate landscape evolution timescales (10–1,000 kyr), the model effectively incorporates the effects of all of the flows of a given magnitude that occur over dt. Given the long timescales we simulate (400 kyr), the model is representative of event-scale variability.

2.2. Block Delivery, Transport, and Degradation

The model's hillslope parameterization recreates the consistently observed positive relationship between river incision, steepening of adjacent hillslopes, and accelerated sediment delivery (in this case, focusing on the accelerated delivery of blocks; e.g., Bennett et al., 2016; Bigi et al., 2006; Gallen et al., 2011; Glade & Anderson, 2018; Glade et al., 2017, Golly et al., 2017; Korup, 2006; Riebe et al., 2015). The mean block flux to the channel per unit channel length per time $\overline{q}_b$ is the product of the mean number of blocks delivered per unit channel length per time $\overline{N}_b$ and the mean block volume $\overline{V}_b$:

$$\overline{q}_b = \overline{N}_b \overline{V}_b. \tag{7}$$

The blocks being delivered to the channel are of a uniform size D_0, implicitly assuming that their size is set by the inherent strength and fracture density of the hillslope bedrock (DiBiase et al., 2018) and that their time spent in the hillslope "weathering engine" is short enough that their size is not reduced significantly (Sklar et al., 2016). Assuming cubic blocks such that each individual block volume V_b is D_0^3,

$$\overline{q}_b = \overline{N}_b D_0^3. \tag{8}$$

The average delivery rate of blocks per unit channel length, $\overline{N}_b$, depends on the time-averaged channel incision rate $\bar{\varepsilon}_c$ along a given channel length and a factor γ. γ, which has dimensions of L^{-2}, describes the efficiency

of hillslope block delivery in response to channel incision. The volume flux of rock to the channel per unit channel length per time is therefore

$$\bar{q}_b = \bar{\varepsilon}_c \gamma D_0^3, \tag{9}$$

where $\bar{\varepsilon}_c$ is the vertical channel erosion rate averaged over a hillsloperesponse timescale T_r to account for the lag time between channel incision and the associated hillslope response. T_r can be estimated from relationships between erosion rate and hillslope response time (e.g., Fernandes & Dietrich, 1997; Hurst et al., 2012) and depends on hillslope length, substrate properties, and transport process dynamics. Equation (9) describes a positive linear relationship between channel incision and block delivery, expected to occur as a result of hillslope steepening in response to incision. The block delivery efficiency parameter γ encapsulates the relative importance of block release and transport processes; higher γ results in more rapid block delivery to the channel. γ should be influenced by bedrock mineralogy, fracture density, and climatic and biologic variables.

Equations (8) and (9), when combined with the assumption that block delivery may be modeled as a Poisson process, imply that $\overline{N}_b$, the average number of blocks delivered per unit channel length over a time period dt, is

$$\overline{N}_b = \bar{\varepsilon}_c \gamma \, \mathrm{d}t. \tag{10}$$

$\overline{N}_b$ depends on the time-averaged incision rate in the adjacent channel, the block delivery efficiency parameter γ, and the time interval dt. Therefore, the number of blocks delivered to the channel per channel length in any given time step is simply a random number drawn from a Poisson distribution with a mean of $\overline{N}_b$. The use of the Poisson distribution implies that the mean number of blocks delivered at a given channel incision rate is constant through time and that all block delivery events occur independently. The question of event independence in hillslope-block delivery in real landscapes is unclear and likely timescale dependent. In some cases, delivery of one block may be followed by delivery of many others (e.g., Rosser et al., 2007). However, over the long term, delivery of many blocks could lead to supply limitations and reduce future block delivery.

Equations (9) and (10) describe a linear relationship between the time-averaged channel erosion rate and the flux of blocks to the channel. We chose a linear relationship for simplicity, and our approach captures the essence of hillslope steepening and block delivery in response to river incision. It is however possible to imagine several different forms for the relationship between channel erosion rate and hillslope block delivery. For example, block flux may increase as a nonlinear function of hillslope gradient and therefore channel erosion rate (e.g., Roering et al., 1999). Alternatively, hillslopes prone to releasing blocks may do so only by landsliding after a threshold hillslope gradient has been achieved (Bennett et al., 2016; Burbank et al., 1996; Carson & Petley, 1970; Larsen & Montgomery, 2012).

Once blocks are delivered to the channel, the bed cover fraction f_c is calculated by

$$f_c = 1 - e^{-\Sigma A_b} \tag{11}$$

where Σ denotes a summation and A_b is the area covered by each block per unit channel bed area. Such an asymptotic relationship is expected because each additional block delivered is more likely than the previous block to overlap with blocks already in the channel, as expected with the cover effect in smaller sediment fractions (Turowski, 2009; Turowski et al., 2007).

The model uses a force balance approach following Lamb et al. (2015) to calculate block motion by sliding. The force balance incorporates the forces generated by buoyancy and gravity, drag force, shear stress along the top of the block, and hydraulic lift force (see the supporting information for force balance equations). Once a block is mobilized, it slides a random distance drawn from an exponential distribution with a mean of one grain diameter. This limited transport distance reflects the assumption that because blocks that significantly impede incision will only be moved by large flows and are unlikely to be in suspension, their time in motion and travel distance will be short (though this assumption may break down in the face of especially flashy peak flows [Alexander & Cooker, 2016]). We also tested a rule in which blocks move exactly one grain diameter per movement event rather than a random distance, but this did not noticeably alter model results. In the force balance, we neglect the potential resisting effects of friction between blocks (F_w in the notation of Lamb et al., 2015), because blocks are not densely packed as they are in the plucking problem for which the

balance was developed (Dubinski & Wohl, 2013; Lamb et al., 2015). Moving blocks in the model do not cause wear on the bed, though there is potential for future models to account for macroabrasion (e.g., Chatanantavet & Parker, 2009) by mobilized blocks. We also neglect the potential for blocks to topple (e.g., Baynes et al., 2015; Lamb & Dietrich, 2009).

Block degradation over time due to abrasion and/or fragmentation is proportional to the shear stress on the blocks:

$$\frac{dD}{dt} = -k_{bb}\left(\tau_{\text{block}} - \tau_{cb}\right), \tag{12}$$

where τ_{cb} is the critical shear stress for detaching rock from the blocks. Equation (12) states that block side length is reduced along all axes in proportion to available shear stress. k_{bb} and τ_{cb} are not required to match the in-channel bedrock parameters k_b and τ_c, allowing for exploration of the effects of lithologic contrasts between blocks and the bed. We assume that weathering is secondary to abrasion and fragmentation in controlling block degradation.

2.3. Numerical Implementation

The Blocky River and Knickpoint Evolution (BRaKE) model solves the governing equations in Python using a locally implicit solution following Braun and Willett (2013) with a time step dt of 10 years. In all cases described below, the model was run over a one-dimensional grid of 100 cells with 10-m cell spacing and channel width (dx = 10 m). Run time for all experiments in the sensitivity analysis was 400 kyr. All other model realizations were run to topographic steady state. The initial condition was a uniform channel slope of 0.0001.

3. Sensitivity Analysis Methods

To understand which parameters in the model most strongly control river channel evolution in the presence of hillslope-derived blocks, we use the Morris One-at-a-Time (MOAT) global sensitivity analysis technique to establish the variability in model outcomes attributable to each model parameter (Adams et al., 2014; Campolongo et al., 2007; Jansen, 1999; Morris, 1991; Saltelli & Annoni, 2010; Saltelli et al., 2004, 2008; Temme & Vanwalleghem, 2016). MOAT is an effective parameter screening method for models with high computational cost where large numbers (>100) of model realizations are not feasible (Saltelli & Annoni, 2010). To evaluate the effects of parameter changes, MOAT uses a set of metrics, or measurable model outputs, chosen by the user. The MOAT algorithm calculates two important quantities: (1) the mean magnitude of the effect of each parameter on a given metric, averaged over many model evaluations across the parameter space (the "modified mean"), and (2) the standard deviation of effects, which measures the variability in parameter influence across the parameter space (the "standard deviation"). We used the MOAT algorithm implemented in the Dakota model analysis toolkit distributed by Sandia National Laboratories (Adams et al., 2014). See the supporting information Text S2 for a full description of the MOAT algorithm.

3.1. Model Parameters and Ranges

To conduct a MOAT analysis, the user must set the parameter ranges that define the extents of the model parameter space. Our chosen parameter ranges are given in Table 1. The three fluvial erosion parameters we include in the MOAT analysis are bed erodibility k_b, critical shear stress τ_c, and flow resistance length scale z_0. Three additional parameters govern hillslope block delivery: block delivery efficiency γ, initial block side length D_0, and hillslope response timescale T_r. Block erodibility k_{bb} and block critical shear stress τ_{cb} govern block degradation in the channel. Finally, E is the erosion rate imposed at the reach outlet (i.e., the base-level lowering rate). We provide an extended discussion justifying our parameter ranges in the supporting information Text S3.

3.2. Model Metrics

We plot and report eight model metrics with which to measure sensitivity to parameter changes: total rock volume eroded from the channel bed; final maximum, mean, and standard deviation of elevation; final maximum, mean, and standard deviation of channel slope (slope is calculated from the elevation drop between each node and its downstream neighbor over distance dx = 10 m); and total number of blocks delivered (Figure 2). We focus on three: the total volume eroded, the final mean channel slope, and the final standard deviation of channel slope. Total erosion at a given imposed base-level lowering rate will be greater over a 400-kyr model realization if the influence of blocks on erosion efficiency is minimal and smaller if blocks significantly inhibit erosion. Mean channel slope is predicted to vary directly with the strength of block effects

Table 1
Parameter Ranges Used in Morris One-at-a-Time Analysis

Parameter	Symbol	Unit	Min	Max
Bed erodibility	k_b	$m^2 \cdot year \cdot kg^{-1}$	3×10^{-8}	3×10^{-5}
Bed critical shear stress	τ_c	Pa	10	1,000
Block delivery coefficient	γ	m^{-2}	0	5
Hillslope response timescale	T_r	year	1,000	1,000,000
Erosion rate	E	m/year	0.00001	0.01
Initial block size	D_0	m	1	6
Block erodibility	k_{bb}	$m^2 \cdot year \cdot kg^{-1}$	3×10^{-8}	3×10^{-5}
Block critical shear stress	τ_{cb}	Pa	10	10,000
Roughness length scale	z_0	m	0.01	1.0

as shown in Figure 1. The standard deviation of channel slope is a measure of the reach-scale disequilibrium present in the channel profile. Because the model domain is a channel reach with constant drainage area, a profile fully equilibrated to the imposed erosion rate is linear (e.g., Whipple & Tucker, 1999) and has zero standard deviation of slope. The standard deviation of channel slope in our reach-scale model reflects both (a) transient channel response to base-level lowering and (b) blocks causing alternating sequences of oversteepened reaches and understeepened reaches (Figure 1). Because blocks inhibit channel adjustment to base-level lowering, high values of standard deviation of slope are often caused by a combination of these two factors. It is possible that the relative importance of parameters could be different over different timescales; here we focus on those that dominate over the 400-kyr run time.

4. Sensitivity Analysis Results

We ran 72 model realizations resulting in eight independent evaluations of the sensitivity of each parameter. A simple way to evaluate the results of the MOAT analysis, suggested by Morris (1991), Adams et al. (2014), and Temme and Vanwalleghem (2016), is to plot the modified mean effect against the standard deviation of the effects for each parameter, resulting in a scatter plot for each model evaluation metric used (Figure 2). The higher the mean effect, the greater the influence a parameter has on the model metric. The higher the standard deviation of effects, the more variable a parameter's influence across the parameter space. Figure 2 shows scatter plots for the eight chosen model metrics. For all eight metrics, the three most important parameters are the erosion rate E, the bed erodibility k_b, and the block delivery parameter γ. Initial block size D_0 is the fourth most important parameter for all metrics. The hillslope response timescale T_r and block critical shear stress τ_{cb} are the least important.

The high mean effects of bed erodibility and erosion rate across all metrics (Figure 2) indicate that simple fluvial erosion models, such as the stream power model, effectively capture first-order controls on river incision even when compared to models incorporating more complexity. However, the importance of the block delivery parameter γ and initial block size D_0 suggests that models incorporating block effects may significantly improve model performance for settings with a supply of large blocks. All eight metrics show γ and D_0 to be more important than τ_c, the critical shear stress. The revelation that γ and D_0 are more important than τ_c is evidence that, in landscapes with a supply of blocks, the bed cover and form drag effects of blocks limit the importance of critical shear stress as an erosion parameter when that critical shear stress does not incorporate the erosion-inhibiting effects of blocks. We focus on the importance of γ, which our sensitivity analysis showed to be the most important block-related model parameter (Figure 2), and its interaction with the mean and variability of the discharge distribution.

5. Effects of Blocks on Steady State Channel Morphology

Here we explore block effects on topographic scaling in rivers and show that the erosion-inhibiting effects of blocks are predictable across a wide range of erosion rates. We begin by investigating the scaling between erosion rate and steady state channel slope. Beginning with the stream power erosion rule (e.g., Lague, 2014; Tucker & Hancock, 2010; Whipple & Tucker, 1999):

$$\frac{\partial z}{\partial t} = U - KA^m S^n \tag{13}$$

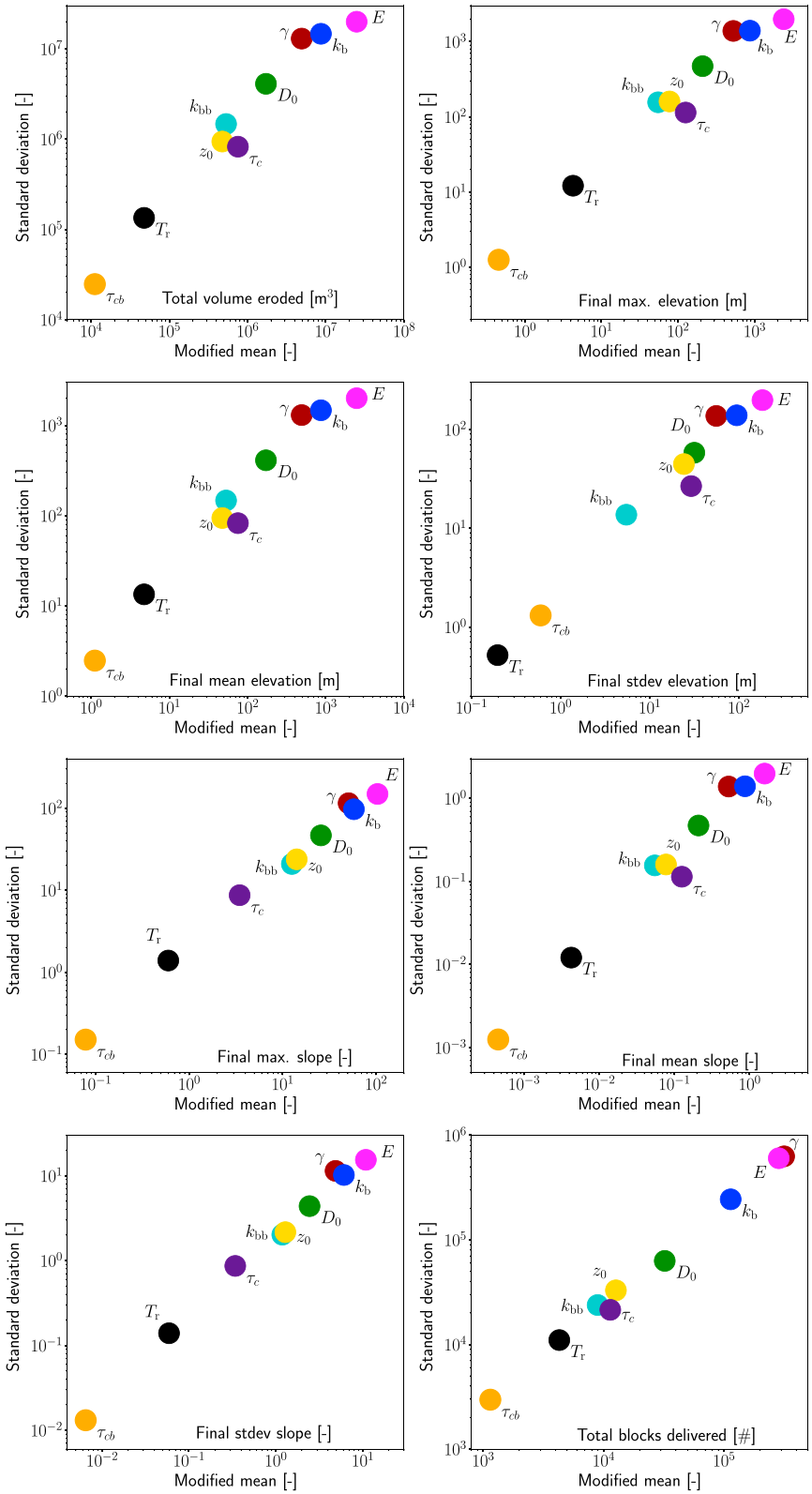

Figure 2. Morris One-at-a-Time results plots for all eight model metrics, with each parameter's mean effect on the *x* axis and standard deviation of effects on the *y* axis. A greater mean effect indicates greater parameter importance, and greater standard deviation indicates nonlinear effects or interparameter interactions. The most important parameters are either standard stream power/shear stress parameters (k_b and E) or block-related parameters (γ, D_0, and k_{bb}), suggesting that block effects are important to channel morphology over a wide range of the parameter space.

where $\frac{\partial z}{\partial t}$ is elevation change per unit time, U is rock uplift relative to base level, K is a bed erodibility coefficient, S is channel slope, and m and n are exponents; it is possible to find an expression for the channel slope at topographic steady state ($\frac{\partial z}{\partial t} = 0$; rock uplift rate U equals erosion rate E). The steady state channel slope is

$$S = \left(\frac{U}{K}\right)^{1/n} A^{-m/n}, \tag{14}$$

which may be rewritten as

$$S = k_s A^{-m/n} \tag{15}$$

where k_s is the channel steepness index ($k_s = \left(\frac{U}{K}\right)^{1/n}$) and m/n is the channel concavity index (e.g., Flint, 1974; Howard, 1980; Kirby & Whipple, 2012; Whipple & Tucker, 1999; Willgoose et al., 1991; Wobus et al., 2006). Much work has examined the relationship between rock uplift relative to base level and steady state k_s (e.g., DiBiase & Whipple, 2011; Kirby & Whipple, 2012; Miller et al., 2013; Safran et al., 2005; Snyder et al., 2000; Wobus et al., 2006) and has shown that

$$k_s \propto E^{\phi}, \tag{16}$$

where ϕ is generally less than 1. ϕ is a topographic variable that is the product of long-term drainage basin evolution and is equal to $1/n$ in long-term upscaled erosion models (DiBiase & Whipple, 2011; Lague, 2014; Lague et al., 2005).

The stream power incision model occupies a continuum defined by two end member models described in detail by Lague (2014): the stochastic threshold model and the constant discharge model. The stochastic threshold model applies when interactions between discharge variability and the erosion threshold dominate channel evolution, and the constant discharge model applies when threshold effects are negligible. It is important to note that the definition of the slope exponent n in the long-term incision model is not the same between these two end members nor at any point along the continuum in between. The stochastic threshold model slope exponent n_s (applicable when the threshold interacts strongly with the discharge distribution) is not equivalent to the constant discharge model slope exponent n_c (applicable when the threshold is negligible) (Lague, 2014). Further, there do not exist analytical expressions for n in the parameter space between the two end member models. Therefore, while ϕ is equal to $1/n$ in long-term upscaled models as long as the definition of n is adjusted appropriately, we focus our discussion on ϕ. We explore the influence of blocks on the scaling of steady state channel slope with erosion rate in our modeled channel reach of uniform drainage area.

5.1. Scaling of Erosion Rate and Steady State Slope

The expected relationship between slope and erosion rate with uniform drainage area and in the absence of block effects is a power law given by equation (14) where A is held constant (so $k_s \propto S$). A plot of erosion rate versus steady state slope (e.g., Figure 3) in log-log space for cases with no block delivery shows a positive, linear relationship with a slope of ϕ. We perform a set of model experiments comparing the no-blocks case ($\gamma = 0$) and cases with $\gamma \neq 0$ and show how changing γ alters the relationship between erosion rate and steady state slope. We also show results for model experiments with four different values of discharge variability c (Figure 3) and mean discharge $\overline{Q}$ (Figure 4).

5.1.1. Influence of Block Delivery on Steady State Slope

Figure 3 shows the effects of changing block delivery efficiency and discharge variability on the relationship between steady state slope and erosion rate. A simple shear stress model with a constant threshold of $\tau_c = 100$ Pa is also shown for comparison. When $\gamma = 0$ (i.e., no blocks), we observe the expected power law relationship between erosion rate and steady state slope and find $\phi \approx 1.35$. A ϕ value of $1 < \phi < 1.5$ is to be expected given the use of a shear stress model formulation (Tucker, 2004; Whipple & Tucker, 1999) combined with the variable power flow resistance equation (Ferguson, 2007). In the constant-threshold case, channel slope is most increased by the threshold at low erosion rates, while the threshold ceases to cause noticeable steepening at high erosion rates.

In every case with block delivery ($\gamma \neq 0$), the steady state mean slope of the channel reach is higher than it is when $\gamma = 0$ for a given erosion rate. In all cases, higher γ results in higher steady state mean slope. Figure 3 shows a transition in model behavior for all values of γ at erosion rates of $\sim 10^{-3}$ m/year. At erosion rates $<10^{-3}$ m/year, the presence of blocks creates up to an order of magnitude increase in steady state slope

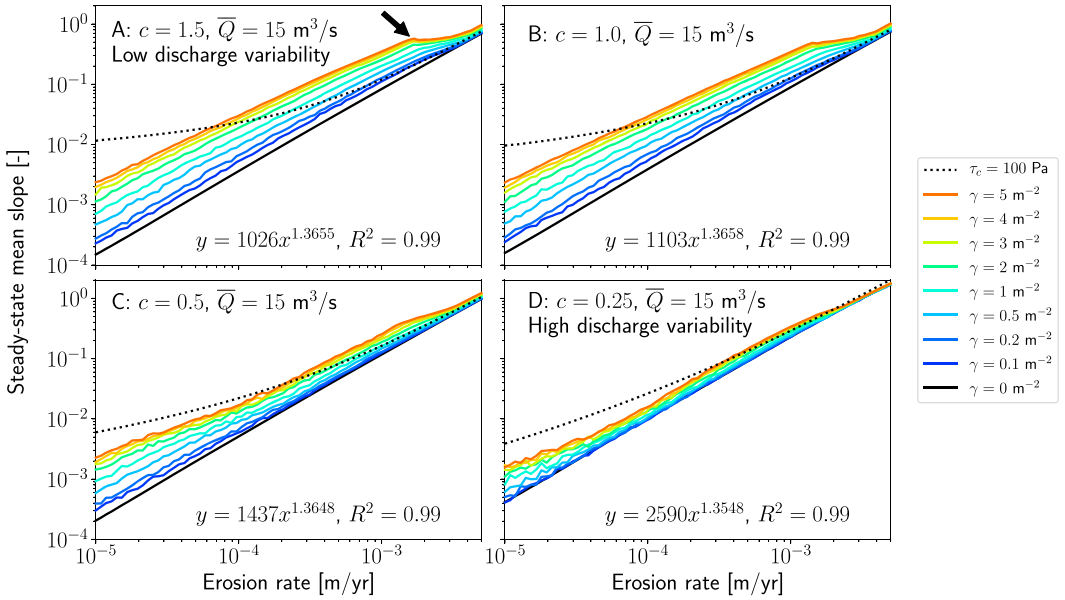

Figure 3. Steady state erosion rate-slope scaling at different values of γ with all other parameters held constant. Each panel shows the results for a different value of c, the discharge distribution shape parameter that governs discharge variability. Each line is made up of 75 model realizations. The black dashed line shows a no-blocks, constant threshold case. Warmer colors show the effects of more efficient block delivery (more blocks delivered for a given channel incision rate). Block delivery can alter steady state slopes by over an order of magnitude, and the magnitude of block influence on slope is set by the discharge variability. All $\gamma \neq 0$ model realizations approach the $\gamma = 0$ case (solid black line and equation) once the channel is able to transport blocks, explaining why the importance of blocks in setting channel slope declines at high erosion rates. An example of the block mobility transition is shown by the black arrow in panel a.

compared to the reference case of no blocks. At erosion rates $>10^{-3}$ m/year, blocks become significantly less effective at increasing steady state slope, and the $\gamma \neq 0$ cases begin to converge toward the $\gamma = 0$ line. As erosion rates continue to increase, even those runs with very efficient block delivery approach the steady state slope of the $\gamma = 0$ case. The transition from the strong influence of blocks on steady state slope at smaller erosion rates to a weakened block influence on slope at greater erosion rates reflects the channel attaining the slope necessary to frequently transport blocks under a given hydrologic regime. The block mobility transition is marked with a black arrow in Figure 3a. Once the channel reaches this threshold slope, blocks become frequently mobile and have fewer incision-inhibiting effects than when they are generally immobile. Figure 3 indicates that the threshold slope is of order 0.3 for the scenarios tested here. While the value of this threshold slope depends strongly on gamma, it also depends on the mean and variability of discharge, which determines the frequency with which blocks move.

5.1.2. Influence of Discharge Variability on Steady State Slope

The influence of block delivery on erosion rate-slope scaling is strongly modulated by discharge variability. The four panels of Figure 3 show model calculations for four different discharge variability scenarios with no change in mean discharge. The discharge variability parameter c controls the relative frequency of large-magnitude streamflow events (e.g., Rossi et al., 2016). Higher values of c yield a more uniform distribution of flows with less-frequent large discharge events, while lower values of c result in a more highly variable discharge distribution. Rossi et al. (2016) analyzed 677 rainfall-dominated gauging stations in the contiguous United States and Puerto Rico with 10–110 years of record and found that c varied between 0.1 and 2.0, with the majority of stations having $0 < c < 1.0$.

When $c = 1.5$ in our lowest variability scenario, block delivery results in steady state slope values up to an order of magnitude larger than the no-blocks case (Figure 3a). The scarcity of large discharge events when $c = 1.5$ results in low block mobility and consequent large increases in steady state channel slope. As c declines to 1.0, 0.5, and 0.25, the relative increase in steady state slope caused by block delivery becomes much smaller (Figures 3b–3d, respectively). When $c = 0.25$, high-magnitude discharge events are frequent enough that blocks are rapidly eroded and transported out of the model domain. In this case, even model runs with very

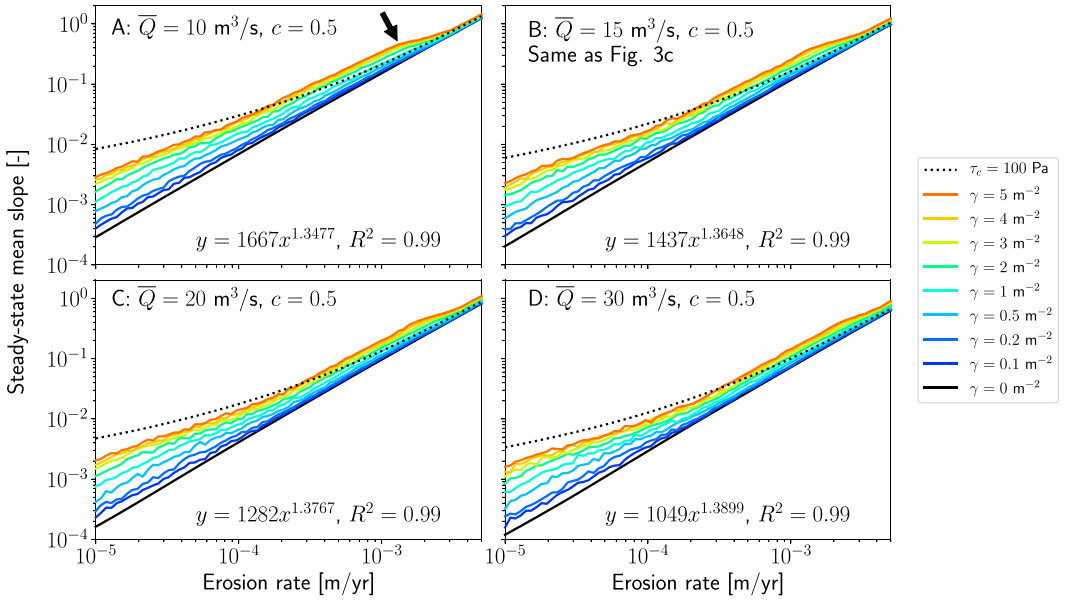

Figure 4. Steady state erosion rate-slope scaling at different values of γ with all other parameters held constant. Each panel shows the results for a different mean discharge $\overline{Q}$. Each line is made up of 75 model realizations. The black dashed line shows a no-blocks, constant threshold case. Discharge variability is held constant at $c = 0.5$. All $\gamma \neq 0$ model realizations approach the $\gamma = 0$ case (solid black line and equation) once the channel is able to transport blocks, indicating that the importance of blocks in setting channel slope declines at high erosion rates. An example of the block mobility transition is shown by the black arrow in panel a. In general, increasing mean discharge reduces the influence of blocks on channel slope, as higher flows allow block transport at lower slopes.

efficient block delivery (i.e., high γ) do not exhibit observable increases in slope relative to the $\gamma = 0$ case (Figure 3). High streamflow variability reduces the distinction between the $\gamma = 0$ and $\gamma = 5$ m^{-2} cases both by raising the steady state slope of the $\gamma = 0$ case and by lowering the steady state slope of the $\gamma \neq 0$ cases. The increase in slope at higher discharge variability when $\gamma = 0$ occurs because flow depth and therefore erosive power increase sublinearly with discharge in the variable power flow resistance equation and would not be observed if erosion rate scaled linearly with discharge. The slopes in the $\gamma \neq 0$ cases decline because of more efficient block degradation and transport due to a higher frequency of large magnitude flows relative to low-variability cases. The other important hallmark of highly variable discharge distributions with respect to block dynamics is that the inflection point at which $\gamma \neq 0$ model runs begin to approach the $\gamma = 0$ case (indicated in Figure 3a by the black arrow) becomes less clear. When $c = 1.5$, the zone of erosion rates within which the $\gamma = 5$ m^{-2} case begins to approach the $\gamma = 0$ case is readily identifiable (Figure 3a). This is the transition zone where the channel slope becomes great enough to transport blocks, such that further increases in block delivery do not significantly impact the steady state channel slope. At lower values of c (more variable discharge distributions), the transition zone from block-influenced morphology to channels so steep that blocks have little effect becomes wider. That is, higher variability in the discharge distribution allows more regular block transport across a wider range of erosion rates.

5.1.3. Influence of Mean Discharge on Steady State Slope

The steepening effects of blocks, as well as the erosion rate at which blocks become mobile and cease to steepen the river profile, depend on the mean discharge. Figure 4 shows the influence of changing γ on channel slope for four different mean discharge values, with the discharge variability held constant at $c = 0.5$. When $\gamma = 0$, slope decreases with increasing mean discharge. In general, higher mean discharge $\overline{Q}$ results in less channel steepening for a given γ relative to the $\gamma = 0$ case. Higher mean discharge leads to a greater proportion of block-mobilizing flows, reducing the steepening effects of hillslope-derived blocks. Together, Figures 3 and 4 show two distinct domains: a range of low erosion rates over which blocks steepen channels significantly and a range of high erosion rates over which block effects appear negligible. Erosion rate interacts with discharge mean and variability to impose self-organized limits on the influence of blocks on channel slope.

5.2. Scaling of Erosion Rate and ϕ

Lague et al. (2005) and DiBiase and Whipple (2011) showed using stochastic threshold incision models with constant erosion thresholds that ϕ is a predictable function of erosion rate E normalized by a threshold term Ψ, where:

$$\Psi = k_b \tau_c^a. \tag{17}$$

They argued that the relationship between E/Ψ and ϕ could be divided into three regimes (DiBiase & Whipple, 2011; Lague et al., 2005). In regime I ($E/\Psi \leq 0.1$), the threshold term is large relative to E, making ϕ the inverse of the stochastic threshold slope exponent n_s, which is set by the variability of the discharge distribution, the at-a-station hydraulic geometry, and the flow resistance relation. In regime III, occurring when the threshold term is negligible relative to E ($10 \leq E/\Psi$), ϕ approaches the inverse of the constant-discharge slope exponent n_c, which is the outcome predicted by stream power and shear stress rules not incorporating a threshold term (Lague, 2014). Regime II ($0.1 \leq E/\Psi \leq 10$) encompasses the transition between these two cases. From the lower to upper end of regime II, the threshold changes from dominating the E-ϕ relationship to becoming negligible as the threshold becomes small relative to E.

In this section we compare the behavior of our block model to the constant-threshold model discussed above. We do not impose a value of τ_c but allow the dynamics of hillslope-derived blocks to determine threshold behavior in the model. It is possible to calculate the effective threshold term Ψ from the block model at steady state by solving for an erosion threshold that is equal to the integrated threshold effects of bed cover and form drag due to all blocks in the channel. At steady state, mean channel reach slope is no longer changing, so the imposed distribution of discharge Q may be transformed into a distribution of flow depths under the simplifying assumption that all slopes are adequately represented by the mean channel reach slope rather than the local slope. Knowing mean block size and spacing from block model results could enable the calculation of dimensionless drag stress σ_D for each flow depth; integrating the effects of blocks on bed cover and drag stress over the full distribution of flow depths (and incorporating the differences between $h > h_b$ and $h \leq h_b$ cases) would then give the effective erosion threshold and Ψ. However, we do not take this approach here. Our parameter space includes cases where the block-induced threshold and therefore Ψ are 0, making the ratio E/Ψ undefined for those cases. We therefore simply plot E rather than E/Ψ against ϕ (Figures 5 and 6). Because we model a channel reach of constant drainage area rather than full channel profiles, we have a direct relationship between slope and erosion rate $S \propto E^{\phi}$. Below, we investigate the influence of block delivery, discharge variability, and mean discharge on the E-ϕ relationship.

5.2.1. Influence of Block Delivery on ϕ

The exponent ϕ governs the shape of the relationship between erosion rate and channel steepness. In Figure 5 we show values of ϕ derived from fitting a line to an 11-point moving window surrounding each point in erosion rate-slope space (Figure 3). The constant-threshold $\tau_c = 100$ Pa case shows an increase in ϕ from $1/n_s$ to $1/n_c$ with increasing erosion rate for all cases, which is consistent with regime II behavior (DiBiase & Whipple, 2011; Lague, 2014; Lague et al., 2005). In the case of a negligible erosion threshold, ϕ approaches the inverse of the constant discharge slope exponent n_c. The $\gamma = 0$ case shows a nearly constant ϕ of ~1.3–1.4 because there is no erosion threshold. When $\gamma \neq 0$, ϕ ranges widely over the tested range of erosion rates.

In general, higher γ values result in lower ϕ for a given erosion rate, though the noise in the data can cause the lines for different γ to overlap (Figure 5). The range of ϕ also increases with increasing γ for a given discharge distribution; ϕ varies only minimally across the erosion rate domain when $\gamma = 0$ but has a range of up to nearly 1.5 for $\gamma = 5$ m^{-2} (Figure 5a). A zone of low ϕ occurs between erosion rates of 1×10^{-3} and 5×10^{-3} m/year, with higher values of γ showing greater departure from their baseline range and ϕ values dipping as low as $\phi \approx 0.2$ (Figure 5). When erosion rates are between 10^{-5} and 10^{-3} m/year, an increase in erosion rate results in an increase in channel slope in response to both the increased erosion rate and any resulting increase in block delivery. When the channel nears a slope that allows transport of blocks, a further increase in erosion rate steepens the channel to the point where blocks are frequently mobile. For this reason, at erosion rates from 1×10^{-3} to 5×10^{-3} m/year, a small increase in channel slope can translate to highly nonlinear increases in erosive power as blocks are removed from the channel bed (i.e., $\phi \ll 1$). The point at which this occurs is marked with a black arrow in Figure 5a. Figure 5 confirms that higher γ model runs show a greater decrease in ϕ than lower γ runs, because higher γ results in more blocks in the channel that may be moved at high enough channel slopes. The block mobility transition, which is unrelated to the three regimes of Lague et al. (2005), separates a zone in which blocks dominate channel evolution (and ϕ) from one in which

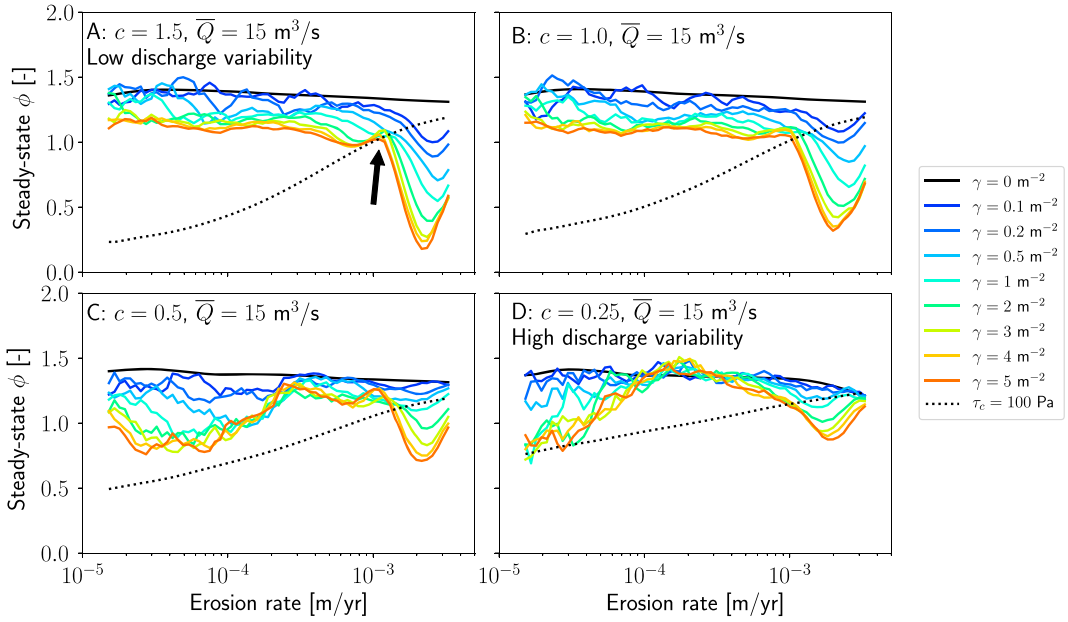

Figure 5. Values of the erosion rate-channel steepness exponent ϕ over the modeled range of erosion rates at different values of γ with all other parameters held constant. Each panel shows the results for a different value of c, the discharge distribution shape parameter. The black dashed line shows a no-blocks, constant threshold case. Mean discharge is held constant at $\overline{Q} = 15$ m^3/s. ϕ is generally lower for higher γ values or higher block-imposed thresholds. When discharge variability is low (high c), ϕ is relatively constant over most of the range of tested erosion rates, before dropping significantly at erosion rates where blocks become frequently mobile. An example of the block mobility transition is shown by the black arrow in panel a. When discharge variability is high (low c), ϕ increases with erosion rate before dropping at the block mobility transition. In all cases, ϕ begins to approach a constant value at very high erosion rates (approaching the regime III behavior of Lague et al., 2005). Discharge variability controls the magnitude of the drop in ϕ at the block mobility transition.

blocks do not noticeably alter channel evolution in comparison to standard stochastic threshold models. We observe substantial differences in ϕ between the block-dominated and non-block-dominated zones across all values of discharge variability and mean discharge (Figures 5 and 6).

5.2.2. Influence of Discharge Variability on ϕ

For large erosion thresholds, the behavior of stochastic threshold models is influenced heavily by the variability of the discharge distribution (DiBiase & Whipple, 2011; Lague, 2014; Lague et al., 2005; Snyder et al., 2003; Tucker, 2004; Tucker & Bras, 2000). DiBiase and Whipple (2011) showed that while discharge variability does not alter predictions of the exponent ϕ when the threshold is negligible compared to the erosion rate (regime III), changing discharge variability significantly alters predictions of ϕ when the threshold is important relative to E (regime I and the lower part of regime II). Here we test the influence of discharge variability on ϕ in our block model by testing $c = 1.5$, 1.0, 0.5, and 0.25 (Figure 5). Higher values of c result in lower discharge variability and vice versa. In the $\gamma = 0$ case, steady state ϕ is effectively constant across the full domain of erosion rates for all values of c (but not exactly constant due to the variable power flow resistance equation). In the $\gamma \neq 0$ cases, low values of c (i.e., high discharge variability) significantly increase the range of ϕ observed at low erosion rates and reduce the range of ϕ at high erosion rates. For a given value of γ, low discharge variability ($c = 1.5$, Figure 5a) results in ϕ varying by up to 1 across the whole erosion rate domain, while high discharge variability ($c = 0.25$, Figure 5d) causes the range of ϕ to be restricted to <0.7. This behavior is broadly consistent with that reported by DiBiase & Whipple (2011; their Figure 8) in that their total range of ϕ declines with increasing discharge variability.

Because the erosion rate and the erosion threshold imposed by blocks change simultaneously, and the specific value of the threshold imposed by blocks is unknown, it is not possible to quantitatively place the block model results in the three-regime framework of Lague et al. (2005). However, the fact that discharge variability exerts a strong influence on ϕ implies that the block models considered here occupy regimes I and II, because discharge variability does not influence ϕ in regime III (DiBiase & Whipple, 2011; Lague et al., 2005). At erosion

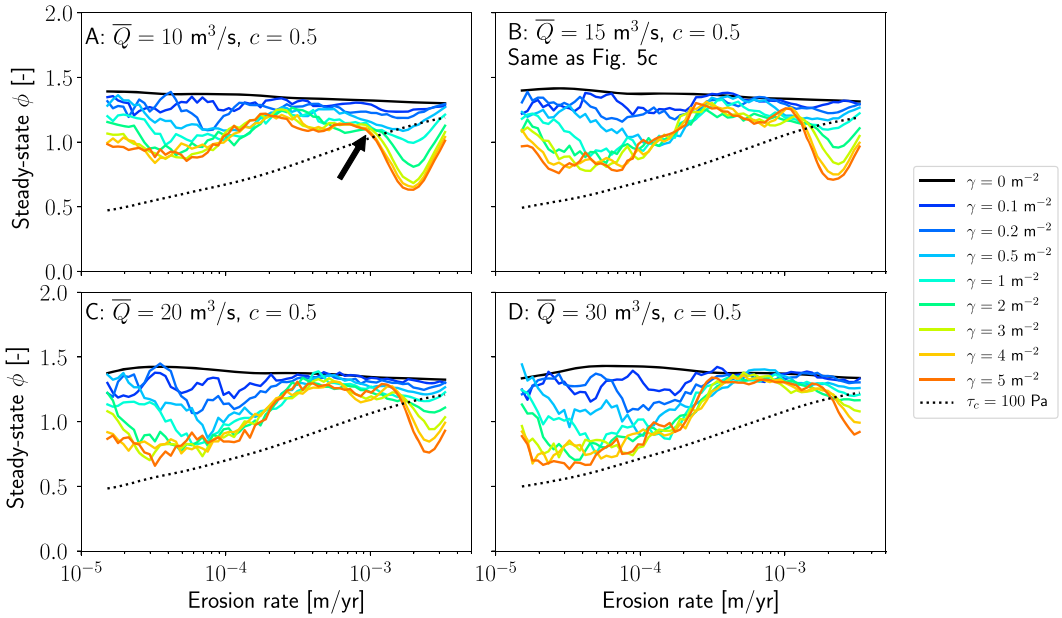

Figure 6. Values of the erosion rate-channel steepness exponent ϕ over the modeled range of erosion rates at different values of γ with all other parameters held constant. Each panel shows the results for a different value of mean discharge $\overline{Q}$. Discharge variability is held constant at $c = 0.5$. The black dashed line shows a no-blocks, constant threshold case. Increasing mean discharge causes (1) increased differences in ϕ between the $\gamma = 0$ and $\gamma \neq 0$ cases at low erosion rates and (2) decreased differences in ϕ between the $\gamma = 0$ and $\gamma \neq 0$ cases at high erosion rates. Both trends are the result of increased block mobility in larger flows. An example of the block mobility transition is shown by the black arrow in panel a. In all cases, ϕ reaches a local maximum at $E \approx 0.001$ m/year before blocks become frequently mobile and result in a drop in ϕ.

rates far above the block mobility transition, the threshold imposed by the blocks declines in importance relative to the erosion rate and we observe an approach toward regime III behavior. Figure 5d shows that when discharge variability is high, the different γ cases begin to converge toward a single ϕ value and would likely reach this value at erosion rates higher than those we examined. However, the influence of discharge variability on ϕ at high erosion rates (Figure 5) shows that the block mobility transition does not itself represent a change to regime III.

Our results provide insight into the transition zone (erosion rate of ~10^{-3} m/year in Figures 3 and 5, shown by the black arrow in Figures 3a and 5a) between the region of erosion rates within which increases in γ cause increased steady state slope (<10^{-3} m/year) and the region in which increasing γ has less of an influence on slope (>10^{-3} m/year). This transition zone is caused by the onset of frequent block mobility and is not equivalent to a change between the regimes of Lague et al. (2005). The change in the exponent ϕ across that transition is larger when γ is greater (Figure 5) but is also strongly influenced by discharge variability. Low discharge variability (high c) produces the greatest contrast in ϕ across the transition because the low variability makes the channel most sensitive to the erosion-inhibiting effects of blocks (Figure 5a). In contrast, high variability (low c) effectively blurs the transition between the two regions by enabling the channel to more frequently mobilize blocks at lower slopes (Figure 5d). The transition-blurring effect of highly variable discharge distributions is especially noticeable when $\gamma \gg 0$ (Figure 5d). The influence of c on ϕ variability across the block mobility transition illustrates that discharge variability sets whether or not block dynamics produce pronounced changes in ϕ across a range of erosion rates.

5.2.3. Influence of Mean Discharge on ϕ

All four values of mean discharge ($\overline{Q}$) tested show broadly similar behavior for the E-ϕ relationship (Figure 6). When $\gamma \neq 0$, the exponent ϕ broadly increases with increasing erosion rate between erosion rates of 10^{-5} and 10^{-3} m/year, though there is an initial drop in ϕ at higher values of $\overline{Q}$. A drop in ϕ follows, beginning at ~10^{-3} m/year; ϕ then increases toward its $\gamma = 0$ value at high erosion rates. Mean discharge sets the difference in ϕ between the $\gamma \neq 0$ and $\gamma = 0$ cases. Increasing mean discharge, like increasing discharge variability, acts to change ϕ in different ways at different erosion rates. At low erosion rates (~10^{-5} m/year), ϕ at all values

of mean discharge tends to be much lower when $\gamma \neq 0$ than when $\gamma = 0$ (Figure 6). Increasing $\overline{Q}$ causes the difference in ϕ between $\gamma = 0$ and $\gamma \neq 0$ at low erosion rates to grow. The difference is ~0.5 when $\overline{Q} = 10\ m^3/s$ (Figure 6a) and is ~1 when $\overline{Q} = 30\ m^3/s$ (Figure 6d). This drop in ϕ with increasing $\overline{Q}$ at low erosion rates reflects the increasing erosive power of higher $\overline{Q}$.

While at low erosion rates increases in $\overline{Q}$ cause increasing differences in ϕ between the $\gamma \neq 0$ and $\gamma = 0$ cases, increasing $\overline{Q}$ reduces the differences in ϕ at higher erosion rates ($>1 \times 10^{-3}$ m/year). Contrasting Figures 6a and 6d reveals that the difference in ϕ between the $\gamma = 0$ and $\gamma = 5\text{-}m^{-2}$ cases shrinks from ~ 0.75 to ~ 0.5 over a 20 m^3/s increase in $\overline{Q}$. This occurs for the same reason that this drop in ϕ is damped by high discharge variability (Figure 5); the increased prevalence of block-moving flows relative to lower $\overline{Q}$ reduces the difference in ϕ between different block delivery scenarios. Mean discharge, discharge variability, and block delivery predictably interact to set the differences between the block-dominated domain ($E < 10^{-3}$ m/year) and the non-block-dominated domain ($E > 10^{-3}$ m/year). In the next section, we describe how the erosion-inhibiting effects of blocks may be incorporated into existing stochastic threshold models for river evolution.

6. Hillslope-Derived Blocks as an Erosion Threshold: The Variable-Threshold Model

Previous studies have examined the presence and implications of erosion thresholds in bedrock river channels (e.g., Deal et al., 2018; DiBiase & Whipple, 2011; Lague, 2014; Lague et al., 2005; Scherler et al., 2017; Snyder et al., 2003; Tucker, 2004; Tucker & Bras, 2000). Thresholds are commonly expressed as a critical shear stress or critical stream power that must be exceeded for erosion to occur. Quantifying such thresholds can be challenging because thresholds may be imposed by different processes, or combinations of processes, in different natural systems. The relevant threshold may be the stress required to induce incipient motion of bed load (Buffington & Montgomery, 1997), pluck blocks from the channel bed (Lamb et al., 2015; Whipple et al., 2000), or transfer enough energy from saltating bed load to the channel bed to abrade bedrock (Sklar & Dietrich, 2004). For the case of hillslope-derived blocks, we hypothesize that the major threshold setting the transition between block-dominated and non-block-dominated channels is the stress required to mobilize blocks that have been deposited on the channel bed. This is the threshold for block sliding in the Shobe et al. (2016) model but could also be a block toppling threshold (e.g., Baynes et al., 2015; Lamb & Dietrich, 2009). Below that threshold, blocks reduce bed erosion through both bed cover and form drag (Shobe et al., 2016). These effects impose an effective threshold stress needed to keep pace with erosion that is well below the threshold for block mobility. We hypothesize that the effects of blocks on channel form (Figures 3–6) may be effectively parameterized as an erosion threshold. The threshold effects of blocks exist in addition to any other thresholds in the system such as plucking or bed load mobilization thresholds.

River erosion thresholds are generally treated as constant through space and time. Nevertheless, there are a few field sites where prior studies have argued for the need for a variable threshold (Gran et al., 2013; Scherler et al., 2017; Snyder et al., 2003). Snyder et al. (2003) estimated variable critical shear stresses along streams in the Mendocino Triple Junction region, and Gran et al. (2013) used a downstream increase in median grain size (and therefore downstream decrease in Shields stress) to account for down-section coarsening in a glacial till unit. Scherler et al. (2017) incorporated two sources of variability for the threshold of motion for bed load in the Himalaya and Tibet. First, they used a positive relationship between critical Shields stress and channel slope derived by Lamb, Dietrich, & Venditti (2008). Second, they incorporated a power law dependence of median grain size on channel steepness (their Equation 17), capturing the notion that bed load grain size generally increases with steepness (e.g., Attal et al., 2015). Scherler et al. (2017) found that incorporating a grain size dependence on channel steepness helped minimize misfit between modeled and measured erosion rates in some locations, though they found that overall misfit did not change substantially. Here we attempt to incorporate the effects of hillslope-derived blocks as a simple variable erosion threshold.

One possible alternative to using a variable-threshold model is to attempt to subsume the erosion-inhibiting effects of blocks into the bed erodibility coefficient k_b. Ouimet et al. (2007) successfully employed such an approach when considering the effects of landslide dams on river incision on the Tibetan Plateau. However, critical shear stress is a measurable quantity with defined units and a clear physical basis in rivers, whereas k_b is a collection of empirical constants related to local hydrology, sediment flux, and climatic conditions (e.g., Whipple, 2004). There is a theoretical basis for calculating the shear stress required to mobilize blocks of a given size when channel slope and flow conditions are known (Alexander & Cooker, 2016; Carling & Tinkler,

1998; Lamb et al., 2015; Larsen & Lamb, 2016). We prefer the variable-threshold approach because it corresponds physically with the processes governing block mobility.

In the case of hillslope-derived blocks, we expect the threshold experienced by the channel to be set by the frequency of block delivery, which depends linearly on the channel erosion rate. Because hillslope-derived blocks are the source of the erosion threshold in our model, and their delivery is linearly related to the channel erosion rate (equation (10)), we hypothesize that the threshold experienced by the channel should linearly covary with the in-channel erosion rate. Such a dependence of threshold on erosion rate was suggested but not explored by Scherler et al. (2017). While we have asserted a linear relationship between channel incision rate and block delivery (equation (10)), this relationship could take several possible forms as discussed in section 2.2. We focus here on block delivery rate as a control on the erosion threshold, but block size and erodibility also play a role (Dubinski & Wohl, 2013; Lamb et al., 2015) and may also depend on hillslope steepening in response to incision (Attal et al., 2015; Glade et al., 2017; Sklar et al., 2016).

We cast the linear dependence of the block-induced threshold τ_c^{eff} on channel erosion rate as

$$\tau_c^{\text{eff}} = \alpha + \delta E, \tag{18}$$

where α is the critical shear stress at very low erosion rates and δ is a constant of proportionality dependent on block size, block erodibility, and block delivery efficiency γ. Larger blocks, more erosion-resistant blocks, and more efficient block delivery (higher γ) all contribute to higher values of δ or a stronger dependence of τ_c^{eff} on imposed erosion rate. The intercept α depends on block delivery efficiency γ. α approaches 0 when γ is small because low numbers of blocks in the channel make the effective erosion threshold imposed by blocks negligible; α becomes larger as γ increases, because even very low erosion rates trigger delivery of enough blocks to have important threshold effects.

The linear relationship given in equation (18) governs the critical shear stress due to blocks up to the critical erosion rate E_c at which blocks become frequently mobile. As shown in Figures 3–6, above E_c blocks are mobile and therefore no longer act as an erosion rate-dependent threshold, leading to the two separate domains of block effects discussed in section 5. We propose a piecewise function for effective critical shear stress as a function of erosion rate E in which effective critical shear stress increases linearly with E between $E = 0$ m/year and E_c and then remains constant where $E > E_c$ and blocks are frequently mobile:

$$\tau_c^{\text{eff}} = \alpha + \delta E \text{ for } E < E_c \tag{19}$$

and

$$\tau_c^{\text{eff}} = \alpha + \delta E_c \text{ for } E \geq E_c. \tag{20}$$

Equations (19) and (20) describe a new variable-threshold model for block-influenced channels with two distinct domains. The use of a single E_c value is an approximation. Even in our numerical model in which all blocks delivered to the channel have a single initial size, degradation of blocks over time results in a distribution of block sizes in the channel at any given time (Shobe et al., 2016). In reality, block sizes delivered to the channel in a given location may be highly variable, resulting in a transition region of erosion rates separating variable and constant-threshold behavior. We use a single value of E_c here for simplicity to illustrate the behavior of the variable-threshold model.

We estimated α and δ for our block model simulations by minimizing root-mean-square error between the block model slopes and those given by the variable-threshold approximation. Figure 7 shows the contrast between the $\gamma = 0$ case (equivalent to the standard shear stress model with $\tau_c = 0$), the constant-threshold shear stress model with $\tau_c = 100$ Pa (equivalent to a grain diameter of ~0.14 m), and three variable-threshold models where equations (19) and (20) were calibrated to match the block model data. Figure 7 shows that calibrated variable erosion thresholds can reproduce the erosion rate-slope scaling of block-influenced channels at three different nonzero values of γ. Versions of the variable-threshold fit in which the threshold continues to increase or decrease at erosion rates greater than E_c do not fit the block model data as well as a constant threshold at erosion rates above E_c. The variable-threshold parameterizations fit the block model data much more closely than does a constant erosion threshold (Figure 7). Our analysis shows that the significant complexity in the model that treats the delivery, transport, and degradation of hillslope-derived blocks may be subsumed into a variable-threshold approximation that scales τ_c^{eff} linearly with E.

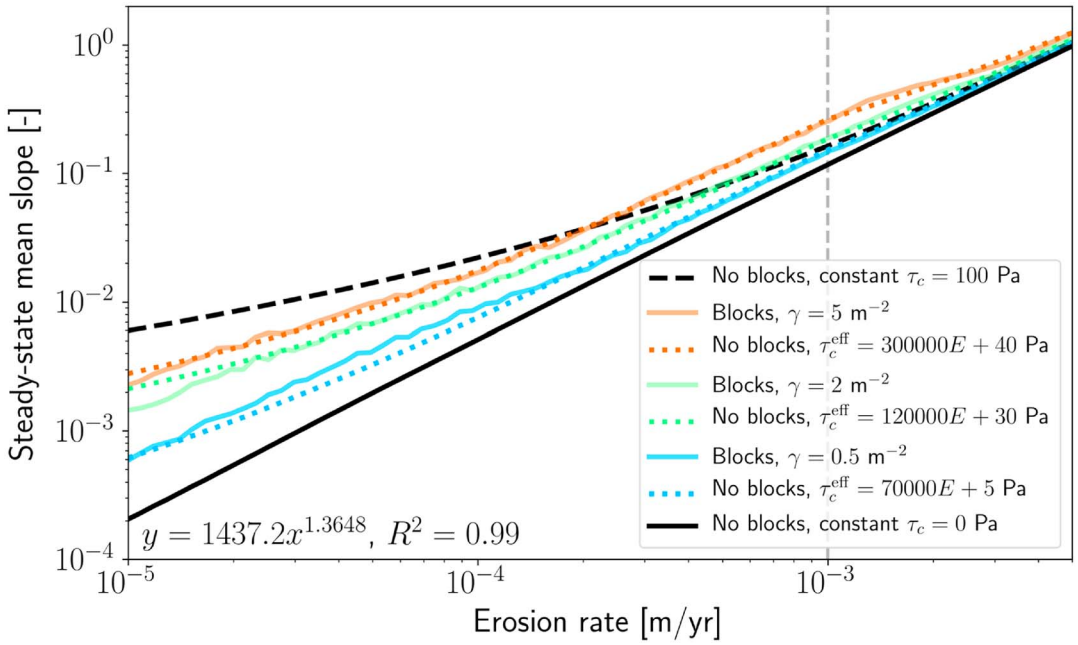

Figure 7. Comparison between topographic outcomes predicted by the standard shear stress model with no erosion threshold and no blocks (solid black line and equation), a standard shear stress model with a constant erosion threshold (dashed black line), the Shobe et al. (2016) model with hillslope block delivery (solid colored lines), and a variable-threshold shear stress model (dotted colored lines). All other parameters were held constant, with mean discharge $\overline{Q} = 15$ m^3/s and discharge distribution shape parameter $c = 0.5$. The vertical dashed gray line separates the variable-threshold and constant-threshold domains of the variable-threshold model fits. The Shobe et al. (2016) block model, as well as our variable-threshold parameterizations, shows distinctly different erosion rate-slope scaling from the no-threshold and constant-threshold cases. The variable-threshold model may be calibrated to fit block model behavior for many different values of γ.

While Figure 7 indicates that the topographic expression of hillslope-derived blocks in channels is well-described by our variable-threshold block model, it does not capture all of the effects of blocks on channel morphology. To illustrate the morphologic differences between the explicit block model and the variable-threshold block model, we compare the two models at two different erosion rates (10^{-5} and 10^{-3} m/year) in Figure 8. The mean slopes of the channel profiles are comparable within 10% between the two models at a given erosion rate, but smaller-scale differences in channel form are noticeable. In the low erosion rate case, the channel in the block model lowers much more rapidly in the first 50 kyr than does the channel in the variable-threshold case. This occurs because the block model incorporates a hillslope response timescale T_r that governs the delay between channel incision and hillslope response, whereas the effective critical shear stress required for erosion in the variable-threshold block model exists at all times. The lack of a delay between river incision and erosion inhibition in the variable-threshold model does not affect our steady state results but could cause differences between the two models in transient cases. In the high erosion rate case, the block model does not reach perfect steady state due to increased loading by blocks with distance downstream. Both of the block model cases exhibit the characteristic local slope deviations or "steps" associated with spatially heterogeneous block delivery. While local-scale differences in profile form between the two models remain, the variable-threshold model effectively reproduces the reach-scale morphology (i.e., mean slope) of the block model.

7. Implications of the Variable-Threshold Model for the Erosion Rate-Channel Steepness Relationship

Many previous studies have attempted to relate long-term erosion rates to channel steepness, with some finding linear relationships ($\phi \approx 1$; e.g., Godard et al., 2014; Safran et al., 2005) and some finding nonlinear relationships ($\phi \neq 1$; e.g., Harel et al., 2016; Harkins et al., 2007; Scherler et al., 2014). Here we explore the implications of our variable-threshold model, in which the block-induced threshold varies with erosion rate,

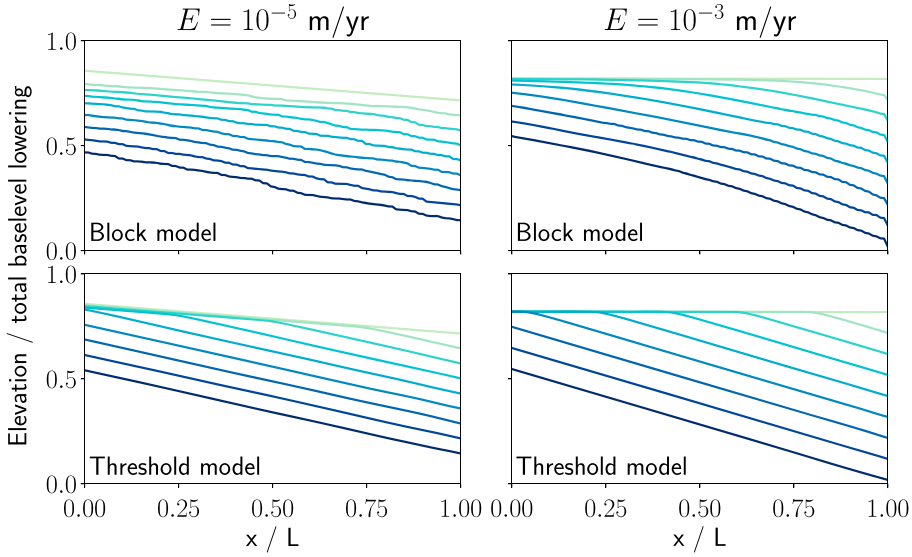

Figure 8. Comparison between time series of reach longitudinal profiles (normalized downstream distance versus normalized elevation) generated by the modified Shobe et al. (2016) block model ($\gamma = 5$ m^{-2}, top) and the variable-threshold model (bottom) at two values of erosion rate. Erosion rate-slope relationships predicted by these two models are shown in the orange solid and dotted lines, respectively, in Figure 7. Profiles are shown evolving over 400 kyr, with profiles plotted every 50 kyr. The variable-threshold model captures mean channel slope but does not generate the local departures from linearity shown by the block model.

for erosion rate-channel steepness scaling and make comparisons to other stochastic-threshold river incision models and field data.

7.1. Influence of the Variable-Threshold Block Model on ϕ

Here we compare the behavior in E-ϕ space of three different parameterizations of the variable-threshold model, each fit to a block model with a different value of γ (Figure 7). Figure 9 shows the relationship between imposed erosion rate E and the erosion rate-channel steepness exponent ϕ for the variable-threshold model calibrated to the $\gamma = 0.5$-, 2-, and 5 m^{-2} cases. We also show the behavior of a no-threshold ($\tau_c = 0$ Pa) and a constant-threshold model ($\tau_c = 100$ Pa). The best-fit α and δ values used to parameterize the $\gamma \neq 0$ fits are given in the legend of Figure 7. The dashed gray line at $E = E_c = 10^{-3}$ m/year in Figure 9 marks the transition zone at which blocks become mobile, below which the variable-threshold block model dictates that τ_c^{eff} increases linearly with erosion rate and above which τ_c^{eff} is asserted to be constant (Figure 7; equations (19) and (20)). The block mobility transition in our model thus marks a change between two distinct types of threshold behavior: threshold increasing linearly with increasing erosion rate and threshold remaining constant with increasing erosion rate. We observe major differences between the variable-threshold block model fits, the no-threshold model, and the constant-threshold model. The no-threshold model shows a small decline in ϕ with increasing erosion rate. The constant-threshold model shows the expected regime II behavior, an increase in ϕ with increasing erosion rate (as opposed to constant low ϕ in regime I or constant high ϕ in regime III). The variable-threshold model parameterizations also show increasing ϕ with increasing erosion rate, aside from the dip in ϕ that occurs at the block mobility transition. Explicit calculation of E/Ψ values for the three variable-threshold model realizations reveals that all fall within regime II, in which the threshold declines in relative importance as erosion rate increases (DiBiase & Whipple, 2011; Lague, 2014; Lague et al., 2005). Above the block mobility transition, ϕ begins to converge to the $\gamma = 0$ value at high erosion rates, indicating that regime III would be reached with continued increases in erosion rate. We do not observe regime I behavior even at the lowest modeled erosion rates because the threshold declines with the erosion rate (equation (19)), continually reducing the importance of threshold effects at low erosion rates.

ϕ in the variable-threshold model depends inversely on the magnitude of the threshold such that higher erosion thresholds lead to lower ϕ. At erosion rates below the transition between variable-threshold and constant-threshold behavior (gray dashed line in Figure 9), ϕ in the variable-threshold models increases with erosion rate. This implies that for the variable-threshold model parameterizations presented here, the relative importance of erosion rate in setting the steady state mean slope increases more rapidly than that of

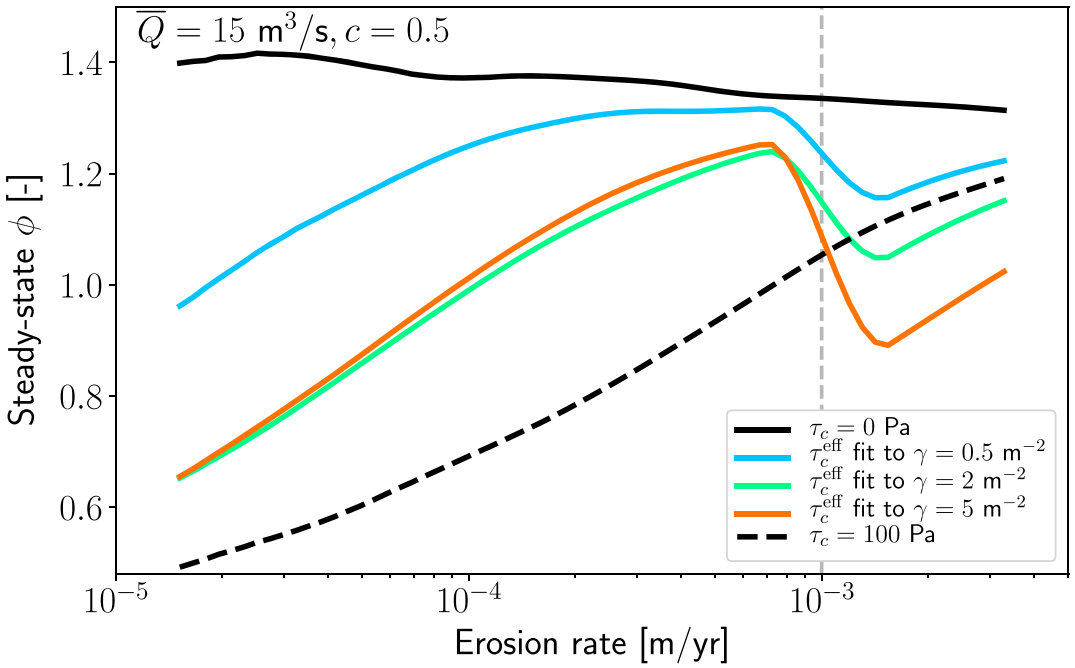

Figure 9. Erosion rate versus ϕ for three variable-threshold model parameterizations in addition to the no-threshold case ($\gamma = 0$, solid black line) and the constant-threshold case ($\tau_c = 100$ Pa, dashed black line). Colors indicate the different variable-threshold model fits from Figure 7. The vertical dashed gray line separates the variable-threshold and constant-threshold domains of the variable-threshold model fits. The most striking difference between our models and standard constant-threshold models, as shown by the explicit block-tracking models in Figure 5, is the drop in ϕ at the transition from an erosion rate-dependent threshold (when blocks tend to be immobile, $E < 0.001$ m/year) to a threshold that is constant and independent of erosion rate (when blocks are frequently mobile, $E > 0.001$ m/year).

the erosion threshold, leading to behavior broadly similar to constant-threshold models. However, the large changes in ϕ surrounding $E = 10^{-3}$ m/year due to the onset of block mobility contrast with the predictions of constant-threshold models, which predict smooth transitions from low ϕ at low erosion rates to high ϕ at higher erosion rates.

The difference in the exponent ϕ across the block mobility transition depends on the variable-threshold parameters α and δ; the no-blocks case shows no change while the $\gamma = 5$ m^{-2} fit shows the greatest change. At erosion rates $>10^{-3}$ m/year where blocks are frequently mobile and the threshold is constant, our variable-threshold model predictably shows behavior similar to that of the constant-threshold model. All three parameterizations of the variable-threshold model appear to be asymptotically approaching constant values of ϕ at erosion rates $>10^{-3}$ m/year, above the block mobility transition. The different parameterizations would all converge to the ϕ value of the $\gamma = 0$ case at higher E values. The ϕ value achieved at the highest erosion rates depends on the magnitude of the threshold; higher thresholds imposed by greater block delivery result in lower ϕ than do smaller thresholds. In summary, the variable-threshold model parameterizations show comparable behavior to the constant-threshold model (DiBiase & Whipple, 2011; Lague et al., 2005) at the upper and lower ends of regime II but differ significantly in that they exhibit a local maximum ϕ followed by a significant drop in ϕ at the transition zone between the variable and constant erosion threshold domains (Figure 9).

7.2. Comparison With the Constant-Threshold Model and Field Data

To enable direct comparison between the proposed variable-threshold model and more common constant-threshold models, we used the channel longitudinal profile evolution model of Lague et al. (2005) to solve for steady state channel steepness for several different constant- and variable-threshold scenarios. It is important to note that the Shobe et al. (2016) block model and the Lague et al. (2005) channel profile evolution differ in their formulation. We used the Lague et al. (2005) model to facilitate comparison of variable thresholds, which may arise from block dynamics, with constant thresholds as explored in previous work (e.g., DiBiase & Whipple, 2011; Lague et al., 2005; Scherler et al., 2017). For the variable-threshold models, we

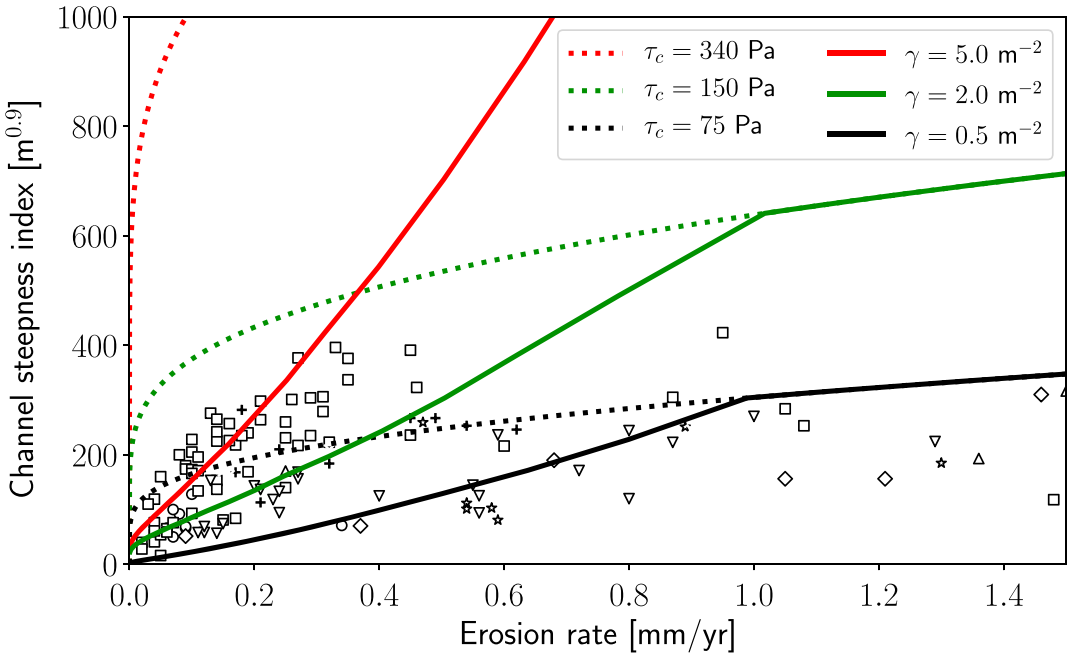

Figure 10. Relationships between erosion rate and channel steepness predicted by the Lague et al. (2005) channel evolution model for three variable-threshold parameterizations (solid lines) compared against relationships produced by constant erosion thresholds (dashed lines). Points are field data compiled by Scherler et al. (2017), with each symbol representing a different study. For all of the cases we explored, the variable-threshold model predicts convex-up $\phi < 1$ behavior at low erosion rates but predicts slightly concave-up $\phi > 1$ behavior over a broad range of erosion rates between ~ 0.1 and 1.0 mm/year. This behavior is consistent with the high ϕ values observed in the block model (Figures 5 and 6) and variable-threshold approximations of the block model (Figure 9). Above the critical block mobility transition ($E = 1$ mm/year), the variable-threshold model transitions to a constant threshold and therefore converges to constant-threshold model behavior. The concavity of E-k_s relationships predicted by the variable-threshold model depends on the strength of the threshold dependence on erosion rate. Data sources are Wobus et al. (2005; stars), Harkins et al. (2007; circles), Finnegan et al. (2008; triangles), Ouimet et al. (2009; squares), Godard et al. (2010; crosses), Godard et al. (2012; diamonds), Godard et al. (2014; inverted triangles), and Scherler et al. (2014; xs).

used the erosion rate-threshold relationships fit to $\gamma = 0.5$-, $\gamma = 2.0$-, and $\gamma = 5.0$ m^{-2} block model data sets (Figure 7) to impose a unique threshold for each erosion rate in the Lague et al. (2005) model. For the constant-threshold models, we ran the Lague et al. (2005) model with a constant threshold equal to the maximum threshold in each of the three variable-threshold cases. We ran the model over a range of erosion rates between 0 and 1.5 mm/year. We also compared both the constant-threshold and variable-threshold predictions to a compilation of field data for the Himalaya and Tibet (Scherler et al., 2017). While we note that the shape and statistics of the discharge distributions in these field locations differ from those used in our model calculations (see Scherler et al., 2017, for an in-depth analysis), the wide variety of field data provides an indication of the natural variability of erosion rate-channel steepness relationships within which any model should fall. Comparisons between the constant-threshold model, variable-threshold model, and field data are shown in Figure 10. Figure 10 represents a simple thought experiment to explore the effects of an erosion rate-dependent threshold, such as could be imposed by block delivery, on channel form. Changes in slope and discharge along a channel profile could change the block-induced threshold in ways that we have not considered here, thus altering predictions for the E-k_s relationship. The parameters used to generate Figure 10 may be found in the supporting information Table S1.

The constant-threshold model parameterizations we tested with the Lague et al. (2005) model predict convex-up relationships between erosion rate and channel steepness ($\phi < 1$, dashed lines on Figure 10). In contrast, the variable-threshold parameterizations in Figure 10 show the same convex-up $\phi < 1$ behavior at low erosion rates before transitioning to very slightly concave-up $\phi > 1$ behavior between erosion rates of ~ 0.1 and 1.0 mm/year. The behavior of variable-threshold parameterizations of the Lague et al. (2005) model echoes the behavior of our block model (Figures 5 and 6) and variable-threshold approximations of the block model (Figure 9) in that ϕ values change with erosion rate but are broadly >1 between 0.1 and 1 mm/year.

The concave-up relationship between erosion rate and channel steepness occurs over a broad range of erosion rates in the variable-threshold model because the greater thresholds at high erosion rates require more channel steepening to achieve steady state than is required for lower thresholds at low erosion rates. As γ increases (i.e., as the threshold increases more rapidly with erosion rate), channels become steeper for a given erosion rate. Importantly however, the variable-threshold model does not exclusively predict E-k_s relationships with $\phi > 1$, just as constant-threshold models do not exclusively predict $\phi < 1$ (e.g., Scherler et al., 2017). A very weak dependence of the threshold on the erosion rate would result in a value of ϕ only slightly lower than the constant-threshold case. The two models converge above the block mobility transition (achieved when $E > 1$ mm/year, Figure 10) as additional block delivery does not force any further increases in effective threshold when blocks are mobile. The point of convergence will vary as a function of block size and delivery rate as well as the discharge distribution.

While the Lague et al. (2005) model was not calibrated to fit the field data shown on Figure 10 for the constant- or variable-threshold cases, both fall within the broad range of the data. It is unlikely that the two models are distinguishable from field observations given the lithological and climatic heterogeneity inherent to drainage basins and the limitations of erosion rates calculated from cosmogenic radionuclide measurements. The best way to test the effectiveness of a variable-threshold model would be to fully calibrate the stochastic-threshold stream power model to a field site and explore whether an erosion rate-dependent threshold helps minimize misfit between measured and modeled E-k_s relationships. DiBiase and Whipple (2011) used such a calibration exercise for the constant-threshold model, and Scherler et al. (2017) attempted to calibrate a variable threshold. Reach-scale calibration of variable thresholds by comparing measured and modeled channel slopes would also be possible using existing data sets (e.g., Johnson et al., 2009).

It is important to recall that the concave-upward ($\phi > 1$) relationship between erosion rate and channel steepness predicted at some erosion rates by the variable-threshold model is a product of (1) the linear relationship between channel incision rate and hillslope block delivery in our block model and (2) the strength of that relationship, set by γ, which determines how strongly the threshold increases with erosion rate. Variable-threshold parameterizations dictating only a very weak dependence of threshold on erosion rate would yield E-k_s curves indistinguishable from the constant-threshold case at all erosion rates. Nonlinear relationships between channel incision and hillslope block delivery, or cases in which block size covaries with delivery rate, could alter the shape of the E-k_s curve predicted by the variable-threshold model. To test for block-induced variable thresholds using field data, it would be necessary to approximate the form of the variable-threshold function by understanding the relationship between channel erosion rate and delivery of material from the hillslopes.

Our analysis reveals two quite different process domains in block-influenced channels: a variable-threshold domain at low erosion rates where blocks are immobile and a constant-threshold domain at high erosion rates when blocks are frequently mobile. We have envisioned a physical mechanism, block delivery, by which the erosion threshold might be intrinsically tied to the erosion rate or rock uplift rate in a basin. An erosion rate-dependent threshold may complicate attempts to extract rock uplift histories from river profiles.

8. Conclusions

We draw four major conclusions from our exploration of a new variable-threshold incision model for block-influenced channels.

1. Hillslope-derived blocks significantly alter river channel evolution across much of the natural parameter space. Block delivery and erodibility exert strong control over channel morphology and evolution. Blocks steepen channels and lead to highly variable local slopes.
2. We observe consistent patterns in the response of channel slope and erosion rate-channel steepness exponent (ϕ) to block delivery, which are set by the competition between block delivery rate, mean discharge, and discharge variability given constant initial block size and erodibility. Specifically, we observe two separate behaviors: Blocks steepen channels at low erosion rates when the blocks are largely immobile, but steepening is reduced at higher erosion rates once blocks are frequently mobile.
3. This dual response to block delivery separates two domains in erosion rate space. At low erosion rates when blocks are immobile, they impose an erosion threshold that scales linearly with erosion rate. At high erosion rates when blocks are mobile, they impose a constant erosion threshold akin to those studied by previous workers.

4. The scaling between erosion rate and channel steepness in our variable-threshold block model is distinct from that predicted by constant-threshold models at erosion rates below the block mobility transition (as long as the threshold varies strongly with erosion rate) but converges with the predictions of constant-threshold models at erosion rates at which blocks are mobile.

Field data sets from Hawaii (Seidl et al., 1994), Utah (Johnson et al., 2009), California (Bennett et al., 2016; DiBiase et al., 2015, 2018), Colorado (Shobe et al., 2016), and Arkansas (Thaler & Covington, 2016) support the idea that the effects of blocks on river evolution described in this paper may be observed in many different climates, lithologies, and tectonic settings. Our results highlight that the interaction between climate and variable erosion thresholds imposed by infrequently mobile sediment can greatly alter the form of fluvially sculpted landscapes. Erosion rate-dependent thresholds may account for more of the observed variability in channel steepness than previously thought. Future work elucidating threshold controls on river erosion is essential to understanding the propagation of tectonic and climatic signals through drainage basins, as well as constraining conditions under which river profiles may be inverted for forcing information.

Notation

A drainage area in stream power incision model
A_b area covered by each block per unit bed area
a incision law exponent
a_1 flow resistance constant
a_2 flow resistance constant
c discharge variability parameter
C_D block drag coefficient
D mean block side length
D_0 initial block side length
E imposed long-term channel erosion rate
f_c fraction of channel bed covered by blocks
g acceleration due to gravity
h flow depth
h_b mean block submergence depth.
K bed erodibility in stream power incision model
k_b bed erodibility in Shobe et al. (2016) model
k_{bb} block erodibility
k_s channel steepness index
m area exponent in stream power incision model
n slope exponent in stream power incision model
$\overline{N}_b$ mean block delivery rate per unit channel length
Q volumetric water discharge
$\overline{Q}$ mean volumetric water discharge
q water discharge per unit channel width
$\overline{q}_b$ mean volumetric block flux to the channel per unit channel length
S channel slope
T_r hillslope response timescale
U rock uplift rate relative to base-level
u_* shear velocity
$\overline{V}_b$ mean block volume
X_0 discharge distribution scale parameter
z_0 roughness length scale
α variable-threshold model parameter
β dimensionless roughness coefficient
γ block delivery coefficient
δ variable-threshold model parameter
ε instantaneous river incision rate
$\overline{\varepsilon}_c$ time-averaged river incision rate
λ mean block spacing

ρ_w water density
σ_D dimensionless drag stress on blocks
τ shear stress
τ_{block} shear stress exerted on in-channel blocks
τ_c critical shear stress for bed erosion
τ_{cb} critical shear stress for block erosion
τ_c^{eff} effective threshold shear stress imposed by blocks
ϕ erosion rate-channel steepness exponent
Ψ threshold term

Acknowledgments
The BRaKE (Blocky River and Knickpoint Evolution) 1.0 model is freely available in the Community Surface Dynamics Modeling System model repository (http://csdms.colorado.edu/wiki/Model:BRaKE). The data and scripts used to generate all figures can be found in the Figshare repository that accompanies this paper (https://doi.org/10.6084/m9.figshare.6082865.v1). This work was supported by NSF EAR-1323137 and EAR-1331828 (the Boulder Creek CZO) to G. E. T. as well as a National Defense Science and Engineering Graduate Fellowship, a University of Colorado Chancellor's Fellowship, and a GSA Fahnestock Award to C. M. S. We thank Bob Anderson and Jason Kean for assistance with model development, Eric Hutton and Mark Piper for help with Dakota, and Peter Molnar, Kelin Whipple, Rachel Glade, Harrison Gray, and Aaron Hurst for helpful discussions. Georgie Bennett, Eric Deal, one anonymous reviewer, and Associate Editor Mikaël Attal provided constructive reviews. We acknowledge computing time on the CU-CSDMS High Performance Computing Cluster.

References

Adams, B. M., Bauman, L. E., Bohnhoff, W. J., Dalbey, K. R., Ebeida, M. S., Eddy, J. P., et al. (2014). Dakota, a multilevel parallel object-oriented framework for design optimization, parameter estimation, uncertainty quantification, and sensitivity analysis: Version 6.0 user's manual (*Sandia Technical Report SAND2014-4633*). Albuquerque, NM, USA): Sandia National Lab. (SNL-NM).

Alexander, J., & Cooker, M. J. (2016). Moving boulders in flash floods and estimating flow conditions using boulders in ancient deposits. *Sedimentology*, *63*, 1582–1595. https://doi.org/10.1111/sed.12274

Anderson, R. S. (1994). Evolution of the Santa Cruz Mountains, California through tectonic growth and geomorphic decay. *Journal of Geophysical Research*, *99*(B10), 20,161–20,179. https://doi.org/10.1029/94JB00713

Attal, M. (2017). Linkage between sediment transport and supply in mountain rivers. In D. Tsutsumi & J. B. Laronne (Eds.), *Gravel-bed rivers: Processes and disasters* (pp. 329–353). UK: John Wiley. https://doi.org/10.1002/9781118971437.ch12

Attal, M., Cowie, P. A., Whittaker, A. C., Hobley, D. E. J., Tucker, G. E., & Roberts, G. P. (2011). Testing fluvial erosion models using the transient response of bedrock rivers to tectonic forcing in the Apennines, Italy. *Journal of Geophysical Research*, *116*, F02005. https://doi.org/10.1029/2010JF001875

Attal, M., & Lavé, J. (2006). Changes of bed load characteristics along the Marsyandi River (central Nepal): Implications for understanding hillslope sediment supply, sediment load evolution along fluvial networks, and denudation in active orogenic belts. *Geological Society of America Special Papers*, *398*, 143–171. https://doi.org/10.1130/2006.2398(09)

Attal, M., Mudd, S. M., Hurst, M. D., Weinman, B., Yoo, K., & Naylor, M. (2015). Impact of change in erosion rate and landscape steepness on hillslope and fluvial sediments grain size in the Feather River basin (Sierra Nevada, California). *Earth Surf Dynamics*, *3*, 201–222. https://doi.org/10.5194/esurf-3-201-2015

Baldwin, J. A., Whipple, K. X., & Tucker, G. E. (2003). Implications of the shear stress river incision model for the timescale of postorogenic decay of topography. *Journal of Geophysical Research*, *108*(B3), 2158. https://doi.org/10.1029/2001JB000550

Baynes, E. R. C., Attal, M., Niedermann, S., Kirstein, L. A., Dugmore, A. J., & Naylor, M. (2015). Erosion during extreme flood events dominates holocene canyon evolution in northeast Iceland. *Proceedings of the National Academy of Science*, *112*(8), 2355–2360. https://doi.org/10.1073/pnas.1415443112

Bennett, G. L., Miller, S. R., Roering, J. J., & Schmidt, D. A. (2016). Landslides, threshold slopes, and the survival of relict terrain in the wake of the Mendocino Triple Junction. *Geology*, *44*(5). https://doi.org/10.1130/G37530.1

Bigi, A., Hasbargen, L. E., Montanari, A., & Paola, C. (2006). Knickpoints and hillslope failures: Interactions in a steady-state experimental landscape. *Geological Society of America Special Papers*, *398*, 295–307. https://doi.org/10.1130/2006.2398(18)

Bonetti, S., & Porporato, A. (2017). On the dynamic smoothing of mountains. *Geophysical Research Letters*, *44*, 5531–5539. https://doi.org/10.1002/2017GL073095

Braun, J., & Willett, S. D. (2013). A very efficient O(*n*), implicit and parallel method to solve the stream power equation governing fluvial incision and landscape evolution. *Geomorphology*, *180–181*, 170–179. https://doi.org/10.1016/j.geomorph.2012.10.008

Buffington, J. M., & Montgomery, D. R. (1997). A systematic analysis of eight decades of incipient motion studies, with special reference to gravel-bedded rivers. *Water Resources Research*, *33*(8), 1993–2029. https://doi.org/10.1029/96WR03190

Burbank, D. W., Leland, J., Fielding, E., Anderson, R. S., Brozovic, N., Reid, M. R., et al. (1996). Bedrock incision, rock uplift and threshold hillslopes in the northwestern Himalayas. *Nature*, *379*, 505–510. https://doi.org/10.1038/379505a0

Campolongo, F., Cariboni, J., & Saltelli, A. (2007). An effective screening design for sensitivity analysis of large models. *Environmental Modelling and Software*, *22*, 1509–1518. https://doi.org/10.1016/j.envsoft.2006.10.004

Carling, P., & Tinkler, K. (1998). Conditions for the entrainment of cuboid boulders in bedrock streams: An historical review of literature with respect to recent investigations. In J. Tinkler & E. Wohl (Eds.), *Rivers over rock: Fluvial processes in bedrock channels* (Vol. 107, pp. 19–33). Washington, DC: Geophysical Monograph, American Geophysical Union.

Carson, M. A., & Petley, D. J. (1970). The existence of threshold hillslopes in the denudation of the landscape. *Transactions of the Institute of British Geographers*, *49*, 71–95.

Chatanantavet, P., & Parker, G. (2008). Experimental study of bedrock channel alleviation under varied sediment supply and hydraulic conditions. *Water Resources Research*, *44*, W12446. https://doi.org/10.1029/2007WR006581

Chatanantavet, P., & Parker, G. (2009). Physically based modeling of bedrock incision by abrasion, plucking, and macroabrasion. *Journal of Geophysical Research*, *114*, F04018. https://doi.org/10.1029/2008JF001044

Cook, K. L., Turowski, J. M., & Hovius, N. (2013). A demonstration of the importance of bed load transport for fluvial bedrock erosion and knickpoint propagation. *Earth Surface Processes and Landforms*, *38*(7), 683–695. https://doi.org/10.1002/esp.3313

Deal, E., Braun, J., & Botter, G. (2018). Understanding the role of rainfall and hydrology in determining fluvial erosion efficiency. *Journal of Geophysical Research: Earth Surface*, *123*, 744–778. https://doi.org/10.1002/2017JF004393

DiBiase, R. A., Rossi, M. W., & Neely, A. B (2018). Fracture density and grain size controls on the relief structure of bedrock landscapes. *Geology*, *46*, 399–402. https://doi.org/10.1130/G40006.1

DiBiase, R. A., & Whipple, K. X. (2011). The influence of erosion thresholds and runoff variability on the relationships among topography, climate, and erosion rate. *Journal of Geophysical Research*, *116*, F04036. https://doi.org/10.1029/2011JF002095

DiBiase, R. A., Whipple, K. X., Lamb, M. P., & Heimsath, A. M. (2015). The role of waterfalls and knickzones in controlling the style and pace of landscape adjustment in the western San Gabriel Mountains, California. *Geological Society of America Bulletin*, *127*(3/4), 539–559. https://doi.org/10.1130/B31113.1

Dubinski, I. M., & Wohl, E. (2013). Relationships between block quarrying, bed shear stress, and stream power: A physical model of block quarrying of a jointed bedrock channel. *Geomorphology*, *180–181*, 66–81. https://doi.org/10.1016/j.geomorph.2012.09.007
Egholm, D. L., Knudsen, M. F., & Sandiford, M. (2013). Lifespan of mountain ranges scaled by feedbacks between land sliding and erosion by rivers. *Nature*, *498*, 475–478. https://doi.org/10.1038/nature12218
Einstein, H. A., & Barbarossa, N. L. (1952). River channel roughness. *Transactions American Society of Civil Engineers*, *117*, 1121–1132.
Ferguson, R. (2007). Flow resistance equations for gravel- and boulder-bed streams. *Water Resources Research*, *43*, W05427. https://doi.org/10.1029/2006WR005422
Ferguson, R. (2012). River channel slope, flow resistance, and gravel entrainment thresholds. *Water Resources Research*, *48*, W05517. https://doi.org/10.1029/2011WR010850
Ferguson, R. (2013). Reach-scale flow resistance. In J. Schroder & E. Wohl (Eds.), *Treatise on geomorphology: Fluvial geomorphology* (Vol. 9, pp. 50–68). New York: Elsevier. https://doi.org/10.1016/B978-0-12-374739-6.00230-X
Fernandes, N. F., & Dietrich, W. E. (1997). Hillslope evolution by diffusive processes: The timescale for equilibrium adjustments. *Water Resources Research*, *33*(6), 1307–1318. https://doi.org/10.1029/97WR00534
Finnegan, N. J., Hallet, B., Montgomery, D. R., Zeitler, P. K., Stone, J. O., Anders, A. M., et al. (2008). Coupling of rock uplift and river incision in the Namche Barwa-Gyala Peri massif, Tibet. *Geological Society of America Bulletin*, *120*(1/2), 142–155. https://doi.org/10.1130/B26224.1
Finnegan, N. J., Klier, R. A., Johnstone, S., Pfeiffer, A. M., & Johnson, K. (2017). Field evidence for the control of grain size and sediment supply on steady-state bedrock river channel slopes in a tectonically active setting. *Earth Surface Processes and Landforms*, *42*(14), 2338–2349. https://doi.org/10.1002/esp.4187
Finnegan, N. J., Sklar, L. S., & Fuller, T. K. (2007). Interplay of sediment supply, river incision, and channel morphology revealed by the transient evolution of an experimental bedrock channel. *Journal of Geophysical Research*, *112*(F3), F03S11. https://doi.org/10.1029/2006JF000569
Flint, J. J. (1974). Stream gradient as a function of order, magnitude, and discharge. *Water Resources Research*, *10*, 969–973.
Gallen, S. F., Wegmann, K. W., Frankel, K. L., Hughes, S., Lewis, R. Q., Lyons, N., et al. (2011). Hillslope response to knickpoint migration in the southern Appalachians: Implications for the evolution of post-orogenic landscapes. *Earth Surface Processes and Landforms*, *36*, 1254–1267. https://doi.org/10.1002/esp.2150
Gasparini, N. M., Bras, R. L., & Whipple, K. X. (2006). Numerical modeling of non-steady-state river profile evolution using a sediment-flux-dependent incision model. *Geological Society of America Special Papers*, *398*, 127–141. https://doi.org/10.1130/2006.2398(08)
Gilbert, G. K. (1877). *Report on the geology of the Henry Mountains*. U.S: Geological Survey Monograph.
Glade, R. C., & Anderson, R. S. (2018). Quasi-steady evolution of hillslopes in layered landscapes: An analytic approach. *Journal of Geophysical Research: Earth Surface*, *123*, 26–45. https://doi.org/10.1002/2017JF004466
Glade, R. C., Anderson, R. S., & Tucker, G. E. (2017). Blocks control hillslope form and persistence of topography in landscapes developed in layered rocks. *Geology*, *45*(4), 311–314. https://doi.org/10.1130/G38665.1
Godard, V., Bourlès, D. L., Spinabella, F., Burbank, D. W., Bookhagen, B., Fisher, G. B., et al. (2014). Dominance of tectonics over climate in Himalayan denudation. *Geology*, *42*(3), 243–246. https://doi.org/10.1130/G35342.1
Godard, V., Burbank, D. W., Bourlès, D. L., Bookhagen, B., Braucher, R., & Fisher, G. (2012). Impact of glacial erosion on ^{10}Be concentrations in fluvial sediments of the Marsyandi catchment, central Nepal. *Journal of Geophysical Research*, *117*, F03013. https://doi.org/10.1029/2011JF002230
Godard, V., Lavé, J., Carcaillet, J., Cattin, R., Bourlès, D., & Zhu, J. (2010). Spatial distribution of denudation in eastern Tibet and regressive erosion of plateau margins. *Tectonophysics*, *491*, 253–274. https://doi.org/10.1016/j.tecto.2009.10.026
Golly, A., Turowski, J. M., Badoux, A., & Hovius, N. (2017). Controls and feedbacks in the coupling of mountain channels and hillslopes. *Geology*, *45*(4), 307–310. https://doi.org/10.1130/G38831.1
Gran, K. B., Finnegan, N., Johnson, A. L., Belmont, P., Wittkop, C., & Rittenour, T. (2013). Landscape evolution, valley excavation, and terrace development following abrupt postglacial base-level fall. *Geological Society of America Bulletin*, *125*(11/12), 1851–1864. https://doi.org/10.1130/B30772.1
Hack, J. T. (1965). Geomorphology of the Shenandoah Valley, Virginia and West Virginia, and origin of the residual ore deposits. *U.S. Geological Survey Professional Paper*, *484*, 88.
Hancock, G. S., Anderson, R. S., & Whipple, K. X. (1998). Beyond power: Bedrock river incision process and form. In K. J. Tinkler & E. Wohl (Eds.), *Rivers over rock: Fluvial processes in bedrock channels, geophysical monograph* (Vol. 107, pp. 35–60). Washington, DC: American Geophysical Union.
Harel, M.-A., Mudd, S. M., & Attal, M. (2016). Global analysis of the stream power law parameters based on worldwide 10Be denudation rates. *Geomorphology*, *268*, 184–196. https://doi.org/10.1016/j.geomorph.2016.05.035
Harkins, N., Kirby, E., Heimsath, A., Robinson, R., & Reiser, U. (2007). Transient fluvial incision in the headwaters of the Yellow River, northeastern Tibet, China. *Journal of Geophysical Research*, *112*, F03S04. https://doi.org/10.1029/2006JF000570
Hobley, D. E. J., Sinclair, H. D., & Cowie, P. A. (2010). Processes, rates, and time scales of fluvial response in an ancient postglacial landscape of the northwest Indian Himalaya. *Geological Society of America Bulletin*, *122*(9–10), 1569–1584. https://doi.org/10.1130/B30048.1
Hobley, D. E. J., Sinclair, H. D., Mudd, S. M., & Cowie, P. A. (2011). Field calibration of sediment flux dependent river incision. *Journal of Geophysical Research*, *116*, F04017. https://doi.org/10.1029/2010JF001935
Howard, A. D. (1980). Thresholds in river regimes. In D. R. Coates & J. D. Vitek (Eds.), *The concept of geomorphic thresholds* (Vol. 9, pp. 227–258). Boston and Binghamton: Allen and Unwin.
Howard, A. D. (1994). A detachment-limited model of drainage basin evolution. *Water Resources Research*, *30*(7), 2261–2285. https://doi.org/10.1029/94WR00757
Howard, A. D., Dietrich, W. E., & Seidl, M. A. (1994). Modeling fluvial erosion on regional to continental scales. *Journal of Geophysical Research*, *99*(B7), 13,971–13,986. https://doi.org/10.1029/94JB00744
Howard, A. D., & Kerby, G. (1983). Channel changes in badlands. *Geological Society of America Bulletin*, *94*, 739–752.
Hurst, M. D., Mudd, S. M., Walcott, R., Attal, M., & Yoo, K. (2012). Using hilltop curvature to derive the spatial distribution of erosion rates. *Journal of Geophysical Research*, *117*, F02017. https://doi.org/10.1029/2011JF002057
Jansen, M. (1999). Analysis of variance designs for model output. *Computer Physics Communications*, *117*, 35–43. https://doi.org/10.1016/S0010-4655(98)00154-4
Johnson, J. P. L. (2014). A surface roughness model for predicting alluvial cover and bed load transport rate in bedrock channels. *Journal of Geophysical Research: Earth Surface*, *119*, 2147–2173. https://doi.org/10.1002/2013JF003000
Johnson, J. P. L., Whipple, K. X., Sklar, L. S., & Hanks, T. C. (2009). Transport slopes, sediment cover, and bedrock channel incision in the Henry Mountains, Utah. *Journal of Geophysical Research*, *114*, F02014. https://doi.org/10.1029/2007JF000862

Kean, J. W., & Smith, J. D. (2004). Flow and boundary shear stress in channels with woody bank vegetation. In S. J. Bennett & A. Simon (Eds.), *Riparian vegetation and fluvial geomorphology* (Vol. 8, pp. 237–252). Washington, DC: Water Science and Application Series https://doi.org/10.1029/008WSA17.

Kean, J. W., & Smith, J. D. (2006). Form drag in rivers due to small-scale natural topographic features: 1. Regular sequences. *Journal of Geophysical Research*, *111*, F04009. https://doi.org/10.1029/2006JF000467

Kean, J. W., & Smith, J. D. (2010). Calculation of stage-discharge relations for gravel bedded channels. *Journal of Geophysical Research*, *115*, F03020. https://doi.org/10.1029/2009JF001398

Kirby, E., & Whipple, K. X. (2012). Expression of active tectonics in erosional landscapes. *Journal of Structural Geology*, *44*, 54–75. https://doi.org/10.1016/j.jsg.2012.07.009

Korup, O. (2006). Rock-slope failure and the river long profile. *Geology*, *34*(1), 45–48. https://doi.org/10.1130/G21959.1

Lague, D. (2010). Reduction of long-term bedrock incision efficiency by short-term alluvial cover intermittency. *Journal of Geophysical Research*, *115*, F02011. https://doi.org/10.1029/2008JF001210

Lague, D. (2014). The stream power river incision model: Evidence, theory, and beyond. *Earth Surface Processes and Landforms*, *39*, 38–61. https://doi.org/10.1002/esp.3462

Lague, D., Hovius, N., & Davy, P. (2005). Discharge, discharge variability, and the bedrock channel profile. *Journal of Geophysical Research*, *110*, F04006. https://doi.org/10.1029/2004JF000259

Lamb, M. P., & Dietrich, W. E. (2009). The persistence of waterfalls in fractured bedrock. *Geological Society of America Bulletin*, *121*(7–8), 1123–1134. https://doi.org/10.1130/B26482.1

Lamb, M. P., Dietrich, W. E., & Sklar, L. S. (2008). A model for fluvial bedrock incision by impacting suspended and bed load sediment. *Journal of Geophysical Research*, *113*, F03025. https://doi.org/10.1029/2007JF000915

Lamb, M. P., Dietrich, W. E., & Venditti, J. G. (2008). Is the critical shields stress for incipient sediment motion dependent on channel-bed slope? *Journal of Geophysical Research*, *113*, F02008. https://doi.org/10.1029/2007JF000831

Lamb, M. P., Finnegan, N. J., Scheingross, J. S., & Sklar, L. S. (2015). New insights into the mechanics of fluvial bedrock erosion through flume experiments and theory. *Geomorphology*, *224*, 33–55. https://doi.org/10.1016/j.geomorph.2015.03.003

Larsen, I. J., & Lamb, M. P. (2016). Progressive incision of the channeled scablands by outburst floods. *Nature*, *538*, 229–232. https://doi.org/10.1038/nature19817

Larsen, I. J., & Montgomery, D. R. (2012). Landslide erosion coupled to tectonics and river incision. *Nature Geoscience*, *5*, 468–473. https://doi.org/10.1038/ngeo1479

Miller, S. R., Sak, P. B., Kirby, E., & Bierman, P. R. (2013). Neogene rejuvenation of central appalachian topography: Evidence for differential rock uplift from stream profiles and erosion rates. *Earth Planet Science Letters*, *369–370*, 1–12. https://doi.org/10.1016/j.epsl.2013.04.007

Morris, M. D. (1991). Factorial sampling plans for preliminary computational experiments. *Technometrics*, *33*(2), 161–174. https://doi.org/10.2307/1269043

Ouimet, W. B., Whipple, K., & Granger, D. E. (2009). Beyond threshold hillslopes: Channel adjustment to base-level fall in tectonically active mountain ranges. *Geology*, *37*(7), 579–582. https://doi.org/10.1130/G30013A.1

Ouimet, W. B., Whipple, K. X., Royden, L. H., Sun, Z., & Chen, Z. (2007). The influence of large landslides on river incision in a transient landscape: Eastern margin of the Tibetan Plateau (Sichuan, China). *Geological Society of America Bulletin*, *119*(11/12), 1462–1476. https://doi.org/10.1130/B26136.1

Riebe, C. S., Sklar, L. S., Lukens, C. E., & Shuster, D. L. (2015). Climate and topography control the size and flux of sediment produced on steep mountain slopes. *Proceedings of the National Academy of Sciences*, *112*(51), 15,574–15,579. https://doi.org/10.1073/pnas.1503567112

Roering, J. J., Kirchner, J. W., & Dietrich, W. E. (1999). Evidence for nonlinear, diffusive sediment transport on hillslopes and implications for landscape morphology. *Water Resources Research*, *35*(3), 853–870. https://doi.org/10.1029/1998WR900090

Rosser, N., Lim, M., Petley, D., Dunning, S., & Allison, R. (2007). Patterns of precursory rockfall prior to slope failure. *Journal of Geophysical Research*, *112*, F04014. https://doi.org/10.1029/2006JF000642

Rossi, M. W., Whipple, K. X., & Vivoni, E. R. (2016). Precipitation and evapotranspiration controls on daily runoff variability in the contiguous United States and Puerto Rico. *Journal of Geophysical Research: Earth Surface*, *121*, 128–145. https://doi.org/10.1002/2015JF003446

Safran, E. B., Bierman, P. R., Aalto, R., Dunne, T., Whipple, K. X., & Caffee, M. (2005). Erosion rates driven by channel network incision in the Bolivian Andes. *Earth Surface Processes and Landforms*, *30*, 1007–1024. https://doi.org/10.1002/esp.1259

Saletti, M., Molnar, P., Hassan, M. A., & Burlando, P. (2016). A reduced-complexity model for sediment transport and step-pool morphology. *Earth Surface Dynamics*, *4*, 549–566. https://doi.org/10.5194/esurf-4-549-2016

Saltelli, A., & Annoni, P. (2010). How to avoid a perfunctory sensitivity analysis. *Environmental Modeling and Software*, *25*, 1508–1517. https://doi.org/10.1016/j.envsoft.2010.04.012

Saltelli, A., Ratto, M., Andres, T., Campolongo, F., Cariboni, J., Gatelli, D., et al. (2008). *Global sensitivity analysis: The primer*. New York: John Wiley.

Saltelli, A., Tarantola, S., Campolongo, F., & Ratto, M. (2004). *Sensitivity analysis in practice: A guise to assessing scientific models*. New York: John Wiley.

Scheingross, J. S., Brun, F., Lo, D. Y., Omerdin, K., & Lamb, M. P. (2014). Experimental evidence for fluvial bedrock incision by suspended and bed load sediment. *Geology*, *42*(6), 523–526. https://doi.org/10.1016/j.geomorph.2015.03.003

Scheingross, J. S., & Lamb, M. P. (2016). Sediment transport through self-adjusting, bedrock-walled waterfall plunge pools. *Journal of Geophysical Research: Earth Surface*, *121*, 939–963. https://doi.org/10.1002/2015JF003620

Scherler, D., Bookhagen, B., & Strecker, M. R. (2014). Tectonic control on 10Be-derived erosion rates in the Garhwal Himalaya, India. *Journal of Geophysical Research: Earth Surface*, *118*, 1–24. https://doi.org/10.1002/2013JF002955

Scherler, D., DiBiase, R. A., Fisher, G. B., & Avouac, J.-P. (2017). Testing monsoonal controls on bedrock river incision in the Himalaya and Eastern Tibet with a stochastic-threshold stream power model. *Journal of Geophysical Research: Earth Surface*, *122*, 1389–1429. https://doi.org/10.1002/2016JF004011

Schneider, J. M., Rickenmann, D., Turowski, J. M., Schmid, B., & Kirchner, J. W. (2016). Bed load transport in a very steep mountain stream (Riedbach, Switzerland): Measurement and prediction. *Water Resources Research*, *52*, 9522–9541. https://doi.org/10.1002/2016WR019308

Seidl, M. A., Dietrich, W. E., & Kirchner, J. W. (1994). Longitudinal profile development into bedrock: An analysis of Hawaiian channels. *Journal of Geology*, *102*, 457–474. https://doi.org/10.1086/629686

Shobe, C. M., Tucker, G. E., & Anderson, R. S. (2016). Hillslope-derived blocks retard river incision. *Geophysical Research Letters*, *43*, 5070–5078. https://doi.org/10.1002/2016GL069262

Shobe, C. M., Tucker, G. E., & Barnhart, K. R. (2017). The SPACE 1.0 model: a Landlab component for 2-D calculation of sediment transport, bedrock erosion, and landscape evolution. *Geoscientific Model Development*, *10*, 4577–4604. https://doi.org/10.5194/gmd-10-4577-2017

Sklar, L. S., & Dietrich, W. E. (1998). River longitudinal profiles and bedrock incision models: Stream power and the influence of sediment supply. In K. J. Tinkler & E. Wohl (Eds.), *Rivers over rock: Fluvial processes in bedrock channels, geophysical monograph* (Vol. 107, pp. 237–260). Washington, DC: American Geophysical Union.

Sklar, L. S., & Dietrich, W. E. (2004). A mechanistic model for river incision into bedrock by saltating bed load. *Water Resources Research*, *40*, W06301. https://doi.org/10.1029/2003WR002496

Sklar, L. S., & Dietrich, W. E. (2006). The role of sediment in controlling steady-state bedrock channel slope: Implications of the saltation-abrasion model. *Geomorphology*, *82*(1–2), 58–83. https://doi.org/10.1016/j.geomorph.2005.08.019

Sklar, L. S., Riebe, C. S., Marshall, J. A., Genetti, J., Leclere, S., Lukens, C. L., et al. (2016). The problem of predicting the size distribution of sediment supplied by hillslopes to rivers. *Geomorphology*, *277*, 31–49. https://doi.org/10.1016/j.geomorph.2016.05.005

Smith, J. D. (2004). The role of Riparian shrubs in preventing floodplain unraveling along the Clark Fork of the Columbia River in the Deer Lodge Valley, Montana. In S. J. Bennett & A. Simon (Eds.), *Riparian vegetation and fluvial geomorphology* (Vol. 8, pp. 71–85). Washington, DC: Water Science and Application Series, https://doi.org/10.1029/008WSA06.

Snyder, N. P., Whipple, K. X., Tucker, G. E., & Merritts, D. J. (2000). Landscape response to tectonic forcing: Digital elevation model analysis of stream profiles in the Mendocino triple junction region, northern California. *Geological Society of America Bulletin*, *112*(8), 1250–1263. https://doi.org/10.1130/0016-7606(2000)112<1250:LRTTFD>2.0.CO;2

Snyder, N. P., Whipple, K. X., Tucker, G. E., & Merritts, D. J. (2003). Importance of a stochastic distribution of floods and erosion thresholds in the bedrock river incision problem. *Journal of Geophysical Research*, *108*(B2), 2117. https://doi.org/10.1029/2001JB001655

Temme, A. J. A. M., & Vanwalleghem, T. (2016). LORICA—A new model for linking landscape and soil profile evolution: Development and sensitivity analysis. *Computers and Geosciences*, *90*, 131–143. https://doi.org/10.1016/j.cageo.2015.08.004

Thaler, E. A., & Covington, M. D. (2016). The influence of sandstone caprock material on bedrock channel steepness within a tectonically passive setting: Buffalo National River Basin, Arkansas, USA. *Journal of Geophysical Research: Earth Surface*, *121*, 1635–1650. https://doi.org/10.1002/2015JF003771

Tucker, G. E. (2004). Drainage basin sensitivity to tectonic and climatic forcing: Implications of a stochastic model for the role of entrainment and erosion thresholds. *Earth Surface Processes and Landforms*, *29*, 185–205. https://doi.org/10.1002/esp.1020

Tucker, G. E., & Bras, R. L. (2000). A stochastic approach to modeling the role of rainfall variability in drainage basin evolution. *Water Resources Research*, *36*(7), 1953–1964. https://doi.org/10.1029/2000WR900065

Tucker, G. E., & Hancock, G. R. (2010). Modelling landscape evolution. *Earth Surface Processes and Landforms*, *35*, 28–50. https://doi.org/10.1002/esp.1952

Tucker, G. E., & Slingerland, R. (1997). Drainage basin responses to climate change. *Water Resources Research*, *33*(8), 2031–2047. https://doi.org/10.1029/97WR00409

Turowski, J. M. (2009). Stochastic modeling of the cover effect and bedrock erosion. *Water Resources Research*, *45*, W03422. https://doi.org/10.1029/2008WR007262

Turowski, J. M. (2018). Alluvial cover controlling the width, slope and sinuosity of bedrock channels. *Earth Surface Dynamics*, *6*, 29–48. https://doi.org/10.5194/esurf-6-29-2018

Turowski, J. M., & Hodge, R. (2017). A probabilistic framework for the cover effect in bedrock erosion. *Earth Surface Dynamics*, *5*(2), 311–330. https://doi.org/10.5194/esurf-5-311-2017

Turowski, J. M., Lague, D., & Hovius, N. (2007). Cover effect in bedrock abrasion: A new derivation and its implications for the modeling of bedrock channel morphology. *Journal of Geophysical Research*, *112*, F04006. https://doi.org/10.1029/2006JF000697

Turowski, J. M., & Rickenmann, D. (2009). Tools and cover effects in bed load transport observations in the Pitzbach, Austria. *Earth Surface Processes and Landforms*, *34*(1), 26–37. https://doi.org/10.1002/esp.1686

Whipple, K. X. (2004). Bedrock rivers and the geomorphology of active orogens. *Annual Review of Earth and Planetary Sciences*, *32*, 151–185. https://doi.org/10.1146/annurev.earth.32.101802.120356

Whipple, K., Forte, A. M., DiBiase, R. A., Gasparini, N. M., & Ouimet, W. B. (2017). Timescales of landscape response to divide migration and drainage capture: Implications for the role of divide mobility in landscape evolution. *Journal of Geophysical Research: Earth Surface*, *122*, 248–273. https://doi.org/10.1002/2016JF003973

Whipple, K. X., Hancock, G. S., & Anderson, R. S. (2000). River incision into bedrock: Mechanics and relative efficacy of plucking, abrasion, and cavitation. *Geological Society of America Bulletin*, *112*(3), 490–503. https://doi.org/doi:10.1130/0016-7606(2000)112<490:RIIBMA>2.0.CO

Whipple, K. X., Snyder, N. P., & Dollenmayer, K. (2000). Rates and processes of bedrock incision by the Upper Ukak River since the 1912 Novarupta ash flow in the Valley of Ten Thousand Smokes, Alaska. *Geology*, *28*(9), 835–838. https://doi.org/10.1130/0091-7613(2000)28<835:RAPOBI>2.0.CO;2

Whipple, K. X., & Tucker, G. E. (1999). Dynamics of the stream-power river incision model: Implications for height limits of mountain ranges, landscape response timescales, and research needs. *Journal of Geophysical Research*, *104*(B8), 17,661–17,674. https://doi.org/10.1029/1999JB900120

Whipple, K. X., & Tucker, G. E. (2002). Implications of sediment-flux-dependent river incision models for landscape evolution. *Journal of Geophysical Research*, 107. https://doi.org/10.1029/2000JB000044

Willgoose, G., Bras, R. L., & Rodriguez-Iturbe, I. (1991). A physical explanation of an observed link area-slope relationship. *Water Resources Research*, *27*(7), 1697–1702. https://doi.org/10.1029/91WR00937

Wobus, C., Heimsath, A. M., Whipple, K. X., & Hodges, K. V. (2005). Active out-of-sequence thrust faulting in the central Nepalese Himalaya. *Nature*, *434*, 1008–1011. https://doi.org/10.1038/nature03499

Wobus, C., Whipple, K. X., Kirby, E., Snyder, N., Johnson, J., Spyropolou, K., et al. (2006). Tectonics from topography: Procedures, promise, and pitfalls. *Geological Society of America Special Papers*, *398*, 55–74. https://doi.org/10.1130/2006.2398(04)

Yager, E. M., Kirchner, J. W., & Dietrich, W. E. (2007). Calculating bed load transport in steep boulder bed channels. *Water Resources Research*, *43*, W070418. https://doi.org/10.1029/2006WR005432

Zhang, L., Parker, G., Stark, C. P., Inoue, T., Viparelli, E., Fu, X., & Izumi, N. (2015). Macro-roughness model of bedrock-alluvial morphodynamics. *Earth Surface Dynamics*, *3*, 113–138. https://doi.org/10.5194/esurf-3-113-2015